OCEANOGRAPHY

# Arctic Ocean sediments as important current and future sinks for marine microplastics missing in the global microplastic budget

Seung-Kyu Kim[1,2]*, Ji-Su Kim[1], So-Young Kim[3], Nan-Seon Song[4], Hyoung Sul La[3], Eun Jin Yang[3]



**To better understand unexpectedly low plastic loads at the ocean's surface compared with inputs, unidentified sinks must be located. Here, we present the microplastic (MP) budget for multi-compartments in the western Arctic Ocean (WAO) and demonstrate that Arctic sediments serve as important current and future sinks for MPs missing from the global budget. We identified an increase of 3% year$^{-1}$ in MP deposition from sediment core observations. Relatively elevated MP abundances were found in seawater and surface sediments around the summer sea ice retreat region, implying enhanced MP accumulation and deposition facilitated by the ice barrier. We estimate 15.7 ± 2.30 × 10$^{16}$ N and 0.21 ± 0.14 MT as total MP loads in the WAO with 90% (by mass) buried in the post-1930 sediments, which exceeds the global average of the current marine MP load. The slower increase in plastic burial versus production implies a lag in plastic delivery to the Arctic, indicating more pollution in the future.**

## INTRODUCTION

Plastic production with an exponential increase rate now stands at ca. 400 million metric tons (MT) per year; it is projected to double by 2040 (*1*, *2*). Growing scientific evidence on the wide-ranging impacts of plastics on all aspects of life on Earth, including human health, biodiversity, ecosystems, and climate change, has led to calls for immediate attention and legally binding measures to end plastic pollution in the near future (*2*, *3*). Given that 1.5 to 4.1% of produced plastic has entered the ocean (*1*, *4*), plastics accumulated in the marine environment could amount to a few hundred megatons. However, global assessments show unexpectedly low loads of 0.014 to 0.27 MT for plastics floating in ocean surface waters (*5*–*7*), implying the presence of unidentified sinks that contain the remaining plastics. Therefore, finding the missing marine plastics remains a fundamental challenge to balance the global plastic budget and to better identify the negative impacts of plastic accumulation.

Ocean sediments have been proposed as a notable sink for marine plastics because plastics can eventually reach the seafloor and may become permanently buried (*8*, *9*). Martin *et al.* (*10*) suggested that the majority (~88%) of plastics that have entered the ocean since 1950 might have accumulated in the form of micro- and mesoplastics in the global ocean sediments, most of which at the continental slope of 200 to 2000 m depths. By contrast, Lebreton *et al.* (*11*) estimated that ~67% of the post-1950 cumulative marine plastic inputs have remained stranded, settled, and/or buried along the global shorelines in the form of macroplastics. These contradictory results indicate that the global ocean plastic inventory still remains uncertain, along with large differences among the suggested annual plastic marine inputs [0.0061 to 15 MT year$^{-1}$; based on mid-point values in each literature of (*4*, *12*–*15*)].

Microplastics (MPs; ≤5 mm in size), even if originally buoyant, can also sink and deposit on the seafloor as a result of biofilm formation (*16*), expulsion as fecal pellets (*17*), or flocculation and sinking as aggregates (*18*). Although most marine MPs have been estimated to remain below the ocean surface layer (OSL) (*19*), it does not mean that all settling MPs reach the ocean floor considering their vertical oscillation in the water column below the OSL (*20*). Therefore, it remains unclear where the bulk of this material lies as the processes governing the distribution of plastics among ocean surfaces, water columns, and deep-sea sediments are highly variable spatially.

While notable amounts of plastic debris may remain along the shorelines at the mid-latitudes (*11*), a substantial fraction, particularly MPs, can also travel to remote regions such as the Arctic via ocean currents (*21*) and wind (*22*). Surface circulation models and field data have predicted that floating plastics traveling along ocean currents would accumulate within the Arctic Polar circle (*21*). The Arctic Ocean, a semiclosed ocean, is extensively covered with seasonally changing sea ice, of which the smallest summer minimum extent on record was 3.6 × 10$^6$ km$^2$ in 2012 (*23*). Recent studies have found the MP contents that are several orders of magnitude greater in sea ice than in the surrounding seawater and thus suggested that Arctic sea ice constitutes a dead end for floating MPs (*24*–*26*). However, sea ice may also serve as a source to redistribute MPs as temporarily entrapped MPs are released in the melting season. Incorporation in sinking (ice-) algal aggregates was proposed as a potential process facilitating the vertical export of MPs (*27*). Widespread emergence of MPs in the Arctic seafloor has been reported (*27*–*31*), including the highest recorded from worldwide benthic sediments (*27*, *30*). These findings suggest that Arctic sediments may be an important sink of MPs. However, limited knowledge exists on the linkage of MPs in Arctic sediments with overlying sea ice and on the fraction of MPs that are buried in Arctic sediments relative to global ocean MP budgets. Thick permanent or perennial sea ice may retard the further dispersal of floating

[1]Department of Marine Science, College of Natural Sciences, Incheon National University, 119 Academy-ro, Yeonsu-gu, Incheon 22012, Republic of Korea. [2]Yellow Sea Research Institute, Incheon National University, 119 Academy-ro, Yeonsu-gu, Incheon 22012, Republic of Korea. [3]Division of Ocean Sciences, Korea Polar Research Institute, Songdomirae-ro, Yeonsu-gu, Incheon 21990, Republic of Korea. [4]Research Institute of Basic Sciences, Incheon National University, 119 Academy-ro, Yeonsu-gu, Incheon 22012, Republic of Korea.
*Corresponding author. Email: skkim@inu.ac.kr

MPs carried by meltwater and ocean currents because ice floes can create physical barriers to floating pollutant movement (*32*, *33*). We thus hypothesize that the delivered MPs may accumulate around the summer sea ice retreat line because of the ice barrier, facilitating greater MP vertical export to the surrounding seabed.

The western Arctic Ocean (WAO) presents the largest summer sea ice loss in the Arctic Ocean (*34*), and it was reported that considerable amounts of MPs were trapped in its seasonal sea ice (*26*). To test our hypothesis, we explored the spatial distribution of MP abundance in surface sediments and seawater collected from latitudinally different regions of the WAO, including the southern ice-free region and northern ice borderline region in the summer. We also extracted MPs from a sediment core sample to identify the historical trend of Arctic plastic input and to assess whether the MPs in the Arctic sedimentary strata trace the world plastic production history. The main objective of this study was to assess whether Arctic Ocean sediments are an important sink of the MPs missing from the global ocean MP budget. To this end, we calculated the inventory of MPs for the multiple compartments of the WAO, including sea ice, seawater, and sediment, and compared the WAO MP stock with the currently proposed global ocean MP stocks. The abundance of MPs, expressed as the number of plastic particles found in samples, is affected by the degree of fragmentation of plastics (thereby the size) and thus is not informative of plastic loads (*26*, *35*). Thereby, the budgeting of MPs for each compartment of the WAO was conducted for both data in number and mass units. All of the experiments were conducted for MPs ≥20 μm in size, which is the common detection limit of Fourier transform infrared spectroscopy (FTIR) (*36*), to avoid the uncertainty caused by different MP size ranges.

## RESULTS

### Synthetic plastic polymers in seawater and sediment samples

A total of 18,784 particles (mean ± SE, 3131 ± 707 per sample) in surface sediment samples and 24,019 particles (4804 ± 1216 per sample) in seawater samples were scanned by FTIR. We found a total of 103 plastic particles (17 ± 4 per sample) in surface sediment samples and 300 plastic particles (60 ± 25 per sample) in water samples. We also identified a total of 139 plastic particles of 21,625 IR-scanned particles in the sediment core sample. Nineteen different synthetic plastic polymer types were identified from the Arctic samples (Fig. 1). Individual plastic particles were classified into nonfibers (a sum of fragments, sheets, and spherules) and fibers according to their geometric shapes (*26*, *37*).

### Spatial distribution of MPs in surface sediment and seawater

MPs were detected in all surface sediment samples, with an overall mean abundance of 854 (± 180) N $kg^{-1}$. Relatively elevated abundances were found at two northern sites in the East Siberian basin (1102 N $kg^{-1}$ at S22 and 1369 N $kg^{-1}$ at S26) and one site on the continental shelf of the Chukchi basin (1183 N $kg^{-1}$ at S12) (Fig. 1A). Two shelf sediments of the southwestern East Siberian basin and one shelf sediment of the Chukchi basin contained relatively lower MP abundances of 793 N $kg^{-1}$ at S14, 331 N $kg^{-1}$ at S23, and 346 N $kg^{-1}$ at S24. This suggests that MPs are widespread on the WAO seafloor from the Arctic gateway in the south to the summer sea ice borderline region in the north. Notably, the two northernmost sites (S22 and S26) around the summer sea ice borderline exhibited relatively high MP contents. There were no significant correlations between MP abundance and environmental variables [water content, porosity, total organic carbon (TOC) content, and water depth] ($P > 0.05$). The average chlorophyll a content in the overlying water column at depths of 0 to 50 m did not show significant correlation with total MPs of 0.02 to 5 mm (Pearson's correlation, $r = 0.63$, $P = 0.18$). However, there was significant correlation with MPs <0.1 mm, which was the dominant size class, accounting for 51 ± 4.7% of total MPs in sediments (Pearson's correlation, $r = 0.84$, $P = 0.035$). Notably, S22, showing the lowest chlorophyll a content, exhibited the lowest fraction of MPs <0.1 mm in the sediment (32%) compared to other sites (43 to 63%), although the sediment contained the third highest total MP contents (table S1 and fig. S1). This indicates that phytoplankton biomass can be an important driver facilitating the settling of small-sized MPs with the high surface-to-volume ratio at least.

The MPs in seawater ranged from 8.21 to 70.4 N $m^{-3}$, showing the highest abundance in W1 near the Arctic gateway (the Bering Strait) and then decreasing by three to nine times in the northern sites (Fig. 1B). However, the water collected from the ice retreat line region (W5) had two- to threefold enriched MP abundance (24.0 N $m^{-3}$) compared with the waters in the southern ice-free regions (8.2 to 11.9 N $m^{-3}$ in W2 to W4). Despite the difference in years and locations for sample collection, the spatial distribution of MPs in seawater was similar to that in the sediment, in that the MP level was not depleted but rather elevated in the northern ice borderline region even though dilution by dispersal was expected. Although the sample size was small ($N = 5$), each sample represents MPs collected through a continuous sampling from a large section (~100 km per sample) during a vessel navigation rather than from a specific site. A similar trend was observed in another study in which seawater MPs were collected using a manta net (see Fig. 1B) (*38*).

Similarity in MP compositions between the two compartments was also found. Polypropylene (PP) in polymers and fragments in geometric shapes were the most abundant types in both the surface sediment and water samples (Fig. 1, C to F). In terms of overall MP particle counts from all surface sediment samples, PP accounted for the largest proportion of polymers (60%), followed by polyethylene (PE; 17%), polyethylene terephthalate (PET; 8%), and others (<5% each); in terms of shape, fragments accounted for 89%, followed by fibers (10%) and sheets (1%) (Fig. 1, C and D). Similarly, MPs in seawater samples were composed of 52% PP, 24% PE, 14% PP-PE copolymer, 5% PET, and <1% other polymers, and 83% was in fragment form, 16% as fibers, and 1% as sheets (Fig. 1, E and F). No spherical MPs were found in either compartment. Individual polymers were mostly present in nonfiber form with proportions of 67 to 100%, while the majority of PET and polyacrylonitrile (PAN) (>50% each) occurred in fibrous form in both sediment and seawater. The polymer composition in fibrous MPs was also consistent for both compartments, wherein PP and PET fibers accounted for 50 and 40% of fibrous MPs in sediment and 53 and 18% in seawater, respectively. Styrene/acrylate copolymer and alkyd resin, which originate from ship paints (*39*), were rarely found in both sediment and seawater. Considering the compositional similarity of MPs in sediment and water, the surface sediments reflect the features of MPs introduced recently into Arctic water. However, unlike the water samples, the sediment samples showed relatively higher PP

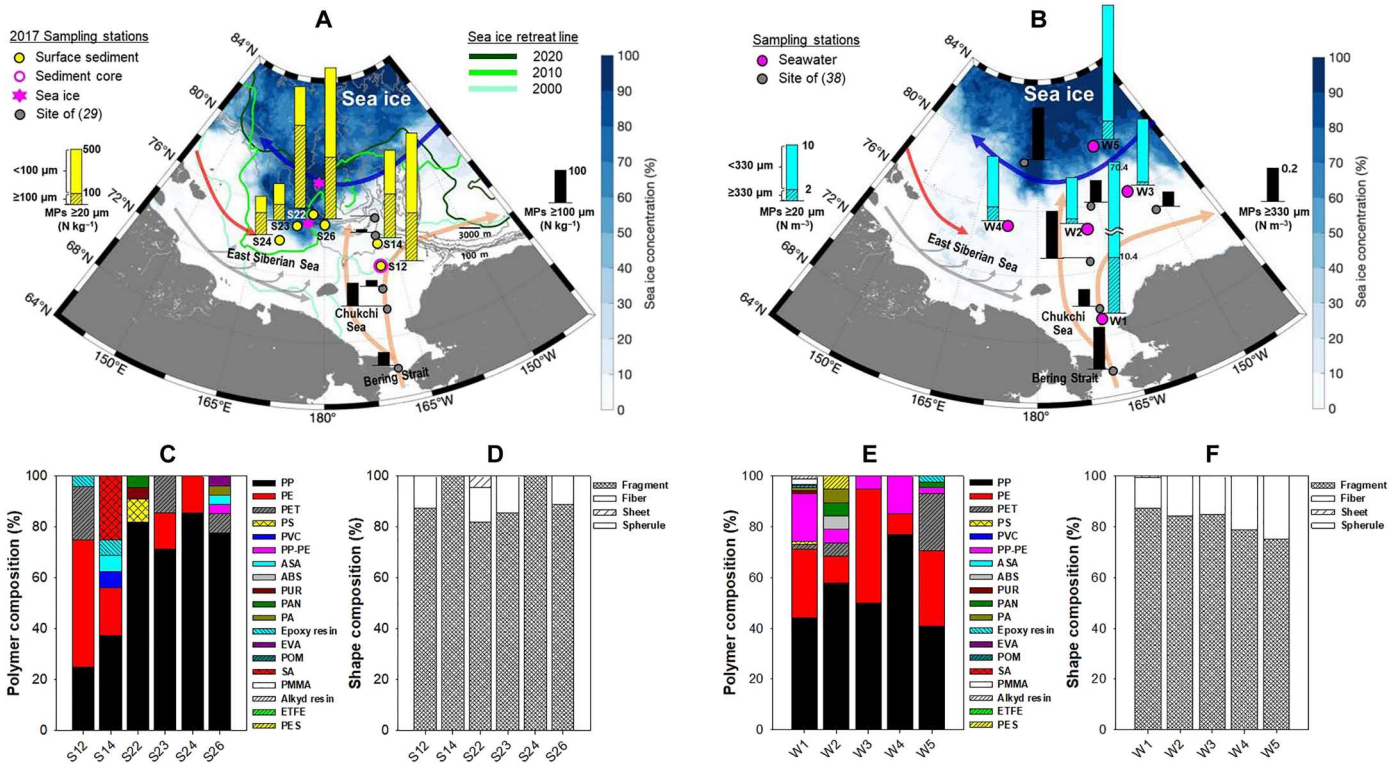


**Fig. 1. Sampling map and spatial distribution of microplastic (MP) content in the western Arctic Ocean (WAO).** (**A**) Sampling sites for surface sediments collected in 2017 and distribution of MP abundance (≥20 µm; yellow bars). (**B**) Sampling sites for seawater collected in 2019 and distribution of MP abundance (≥20 µm; cyan bars). For comparison, sampling sites (gray circles) and MP abundances (black bars) from previous studies with larger MP detection cutoff sizes are illustrated together in (A) for surface sediment (MPs ≥100 µm) (*29*) and in (B) for surface water (MPs ≥330 µm) (*38*), both of which were collected in 2017. Composition profiles of polymers and shapes of MPs ≥20 µm in surface sediment [(**C**) and (**D**), respectively] and seawater [(**E**) and (**F**), respectively]. Sea ice concentration data are for the sampling month (August 2017 for sediment and August 2019 for seawater), and the sea ice retreat lines in (A) represent the data for September in 2000, 2010, and 2020 [NSIDC data based on (*79*, *80*)]. The gray lines refer to the isobaths for 100, 250, 500, 1000, 2000, 3000 m. The arrows in (A) and (B) refer to the Pacific water current (yellow-brown), the Beaufort Gyre flow (blue), the Atlantic water flow (red), and the Siberian coastal current (gray). A sediment core sample was collected at site S12 in (A). PP, polypropylene; PE, polyethylene; PET, polyethylene terephthalate; PS, polystyrene; PVC, polyvinyl chloride; PP-PE, polypropylene-polyethylene copolymer; ASA, acrylonitrile styrene acrylate; ABS, acrylonitrile butadiene styrene; PUR, polyurethane; PAN, polyacrylonitrile; PA, polyamide; EVA, ethylene vinyl acetate; POM, polyoxymethylene; SA, styrene/acrylate copolymer; PMMA, polymethyl methacrylate; ETFE, ethylene tetrafluoroethylene; PES, polyethersulfone.

proportions in the ice borderline region (79 ± 3.1% at S22 to S26) than in the ice-free region (31 ± 6.3% at S12 and S14). The principal components analysis results showed a clear separation of surface sediments into two groups, mostly according to the proportion of PP—ice-free regions (S12 and S14) versus ice-borderline regions (S22 to S26) (fig. S2), compared with the spatially uniform distribution in seawater (54 ± 6.4%). This suggests potentially different MP deposition mechanisms depending on the presence or absence of sea ice in summer and shows accelerated deposition of buoyant PP by sea ice.

## Chronological trend of MP contents in the sediment core

The excess $^{210}$Pb activities ($^{210}Pb_{ex}$) determined from S12 sediment core samples exhibited an exponentially decreasing trend with depths, showing a typical $^{210}$Pb profile—the presence of a surface mixed layer (SML) in the uppermost few centimeters and, below that, a mid-zone with exponential radioactive decay, followed by a lower background zone of constant low activity (Fig. 2A) (*40*–*42*). The radiometrically dated sediment core indicates a distinct physical stratification generated by sediment burial and $^{210}$Pb decay. Thus, the intense biological/physical mixing effect can be ignored except for that in the SML.

MPs were found in every 1-cm transverse layer of the 10-cm-thick sediment core, including the two bottom layers (8 to 9 cm and 9 to 10 cm depth) that were dated to 1942 and 1933, respectively (Fig. 2, B to D). Although there were some variations between different layers, the overall number-based polymer composition was consistent with those in surface sediments and water, with PP and PE accounting for 55% and 23% of the overall MP particles from all layers, respectively, and fibrous MPs mostly consisting of PP (58%) and PET (25%) (fig. S3A). MPs of fragment type were predominant throughout the core (84% in overall MPs and >67% in each layer), which was also analogous to those in surface sediment and seawater (fig. S3B). The bottom two layers, representing the period before the onset of mass production of plastics in the 1950s (*43*), had the lowest MP burial rate. The vertical profile exhibited an exponentially increasing trend in plastic burial over several decades, despite unexpected anomalies in some layers (1979, 1989, and 2012 layers). Multidecadal increases in burial rates of nonfiber and fiber polymers were directly correlated to the worldwide production of

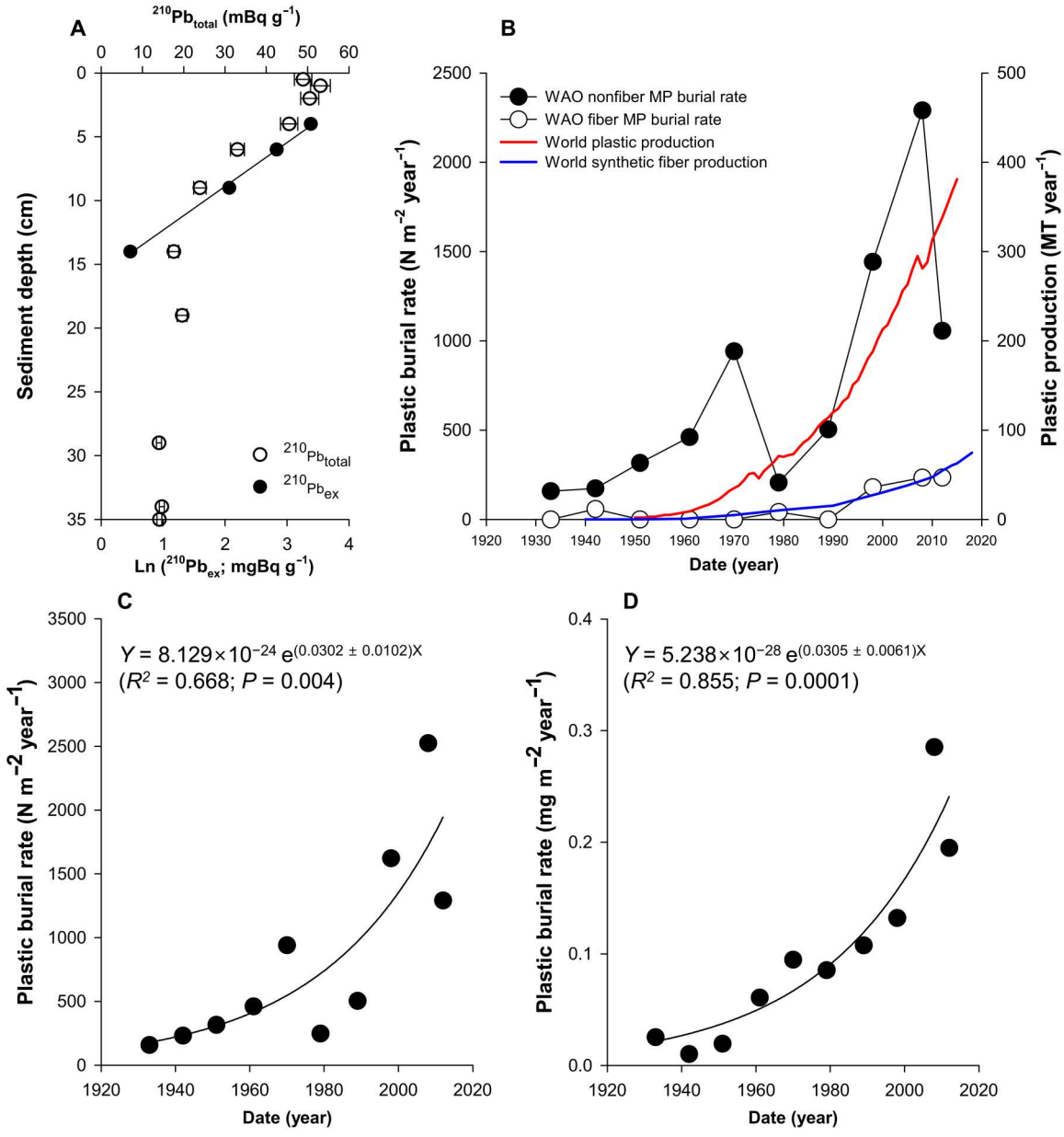


**Fig. 2. Exponential increase of microplastic (MP) deposition in Arctic sediment core.** (**A**) Downcore profile of $^{210}$Pb activities; Linear sedimentation rate (LAR) was determined from the slope of $^{210}Pb_{ex}$ activity versus depth [the linear regression, $Y = -0.29\ (\pm 0.01)\ X + 4.59\ (\pm 0.10)$; $R^2 = 0.997$; $P < 0.01$]. (**B**) Chronological trends in burial rate of nonfiber and fiber MPs were tightly coupled with those in worldwide production of plastics (resin plus fiber) (*1*) and synthetic fibers (*65*), respectively. (**C**) Burial rate of number-based MPs over time (annual rate of increase, 0.0302 ± 0.0102 year$^{-1}$). (**D**) Burial rate of mass-based MPs (nonfibers >0.2 mm in size were excluded) over time (annual rate of increase, 0.0305 ± 0.0061 year$^{-1}$). WAO, western Arctic Ocean; MT, metric tons.

plastic resin (Spearman's ρ = 0.74, $P < 0.05$) and synthetic fiber (Spearman's ρ = 0.65, $P = 0.057$), respectively (Fig. 2B); there were also significant correlations for MP mass burial rates (fig. S4). The burial rates of MPs exhibited significant fits to exponential curves with annual increase rates of 3.02 (± 1.02)% year$^{-1}$ in number ($P < 0.01$; Fig. 2C) and 3.05 (± 0.61)% year$^{-1}$ in mass ($P < 0.001$; Fig. 2D). The average doubling time was 23 years, with a variation of 17 to 35 years and 19 to 28 years, respectively.

The MP burial rate in the sediment core was positively correlated with environmental variables decreasing with depth in the sediment column ($P < 0.01$ for all variables) (fig. S5). Considering a stable chronology and the porosity (~75 to 78%) of sediment strata, the presence of plastics in the pre-1950 layers may be due to the gravity-driven vertical downward transport of MPs through pore water even if the mechanism remains unclear (*44*). The vertical size distribution of MPs revealed that MP particles in pre-1950 layers, although rare, were much smaller and thinner than those in post-1950 layers (Fig. 3). Contamination during sample processing or intense bioturbation, if any, may have resulted in a more random vertical size distribution. Thus, our findings indicate the

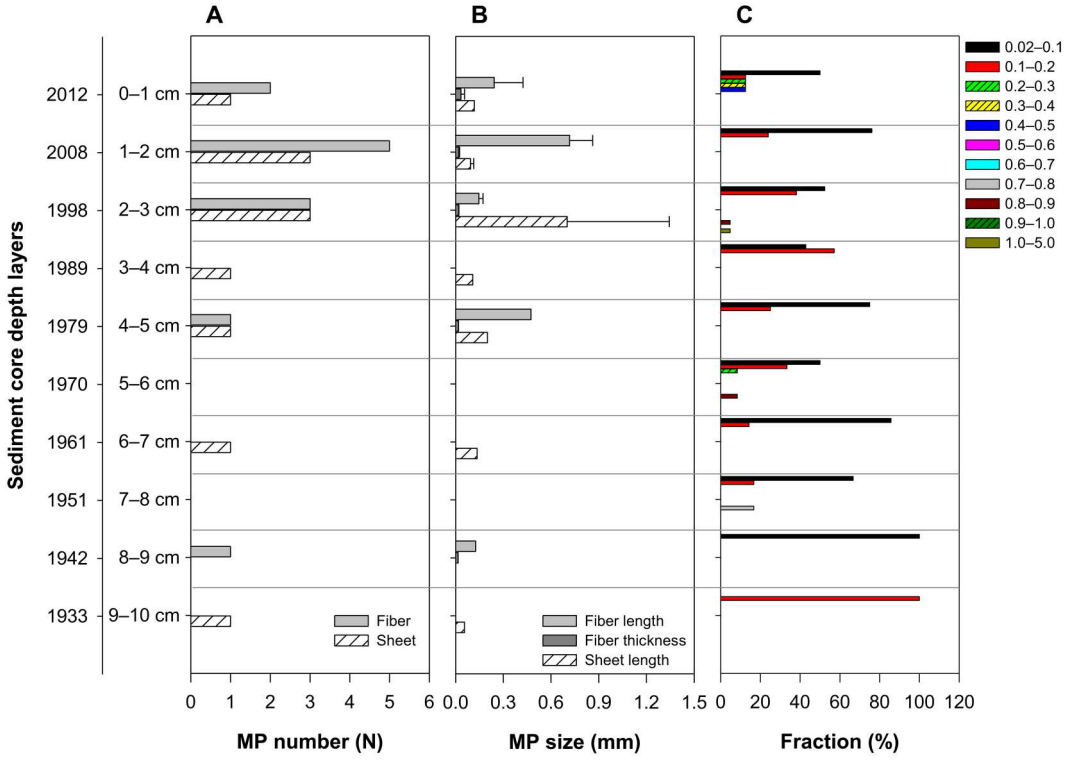


**Fig. 3. Vertical distribution of microplastics (MPs) found in the S12 sediment core.** Depth-dependent changes in the number (**A**) and size (average ± SE) (**B**) of fiber-type (12 pieces) and sheet-type MPs (11 pieces), and in the size distribution of fragment-type MPs (116 pieces) (**C**) show the deficiency in larger-sized MPs in deeper layers. Sizes of MP particles in (B) were larger in the post-1950 layers [0.45 ± 0.11 mm (length) and 0.022 ± 0.004 mm (thickness) for fibers and 0.21 ± 0.004 mm (length) for sheets] than in the pre-1950 layers [0.13 mm (length) and 0.015 mm (thickness) for fiber and 0.056 mm (length) for sheet]. The legend in (C) indicates the size classes (length; mm) of fragment-type MPs in each layer.

possibility of the vertical downward movement of small-sized MPs through pore water even if it was subtle, and also support that any contamination during sample processing and the effects of biological/physical mixing are negligible for MPs accumulated in the S12 sediment core. Unexpected anomalies in MPs in the 1979 and 1989 layers remain unclear considering the distinct sedimentary stratification below the SML. Recently, Kane *et al.* (*45*) suggested that the spatial distribution of MPs in seafloor sediments can be strongly controlled by near-bed thermohaline currents. The WAO has experienced the most rapid changes in geophysical dynamics (ocean circulation) over recent decades; in response to sea ice loss and increased wind mixing, the circulation features of the interior stratified Arctic Ocean, including shelf-break upwelling and Atlantic water intrusion, have changed (*46*–*48*). A change in the thermohaline-driven bottom currents between the late 1970s and early 1990s may have affected seafloor MP accumulation by hindering and/or retarding the stable settlement of MPs, which are more buoyant than soil particles. However, there is no clear evidence to suggest that such geophysical events occurred in the periods around site S12; thus, further study is needed.

## Size effect on number-based MP contents

Only plastic particles below 5 mm were found, with mesoplastics (5 to 25 mm) and macroplastics (>25 mm) not found in either the seawater or sediment samples. Regardless of the sample type, the overall size distributions of MPs (a sum of nonfibers and fibers) showed exponentially increasing trends as the size decreased. Thus, the largest numbers of MPs were present in sizes smaller than 100 μm, accounting for 45, 51, and 58% of MPs in seawater, surface sediment, and sediment cores, respectively. Nonfibers determined the overall MP size distribution, as they comprised 84, 90, and 91% of MPs in the seawater, sediment, and sediment cores, respectively (Fig. 4A). In contrast, fibers were rare below 100 μm: All size classes were represented by light skewing toward the smaller ones (Fig. 4B). Thus, the relative proportion of fibrous MPs gradually increased with increasing size (fig. S6, A to C). This indicates that the shape composition of MPs can be altered according to the detection cutoff size of the measured particles. Size dependency was also observed in polymer composition; the proportion of PP and PE gradually declined from 77% for ≥20 μm to 43% for ≥500 μm in the surface sediment and from 78% for ≥20 μm to 22% for ≥500 μm in the sediment core (fig. S6, D to F). To further assess the effect of the measured cutoff size on MP abundance, available Arctic surface sediment data were compared with respect to different detection sizes (Fig. 5). Sedimentary MP abundances exhibited a significant negative correlation between their logarithmic values and the detection cutoff sizes ($r = 0.965$ and $P < 0.01$), although they were measured in different locations. These findings indicate that the composition and abundance of MPs are critically influenced by the detection cutoff size of the measured particles.

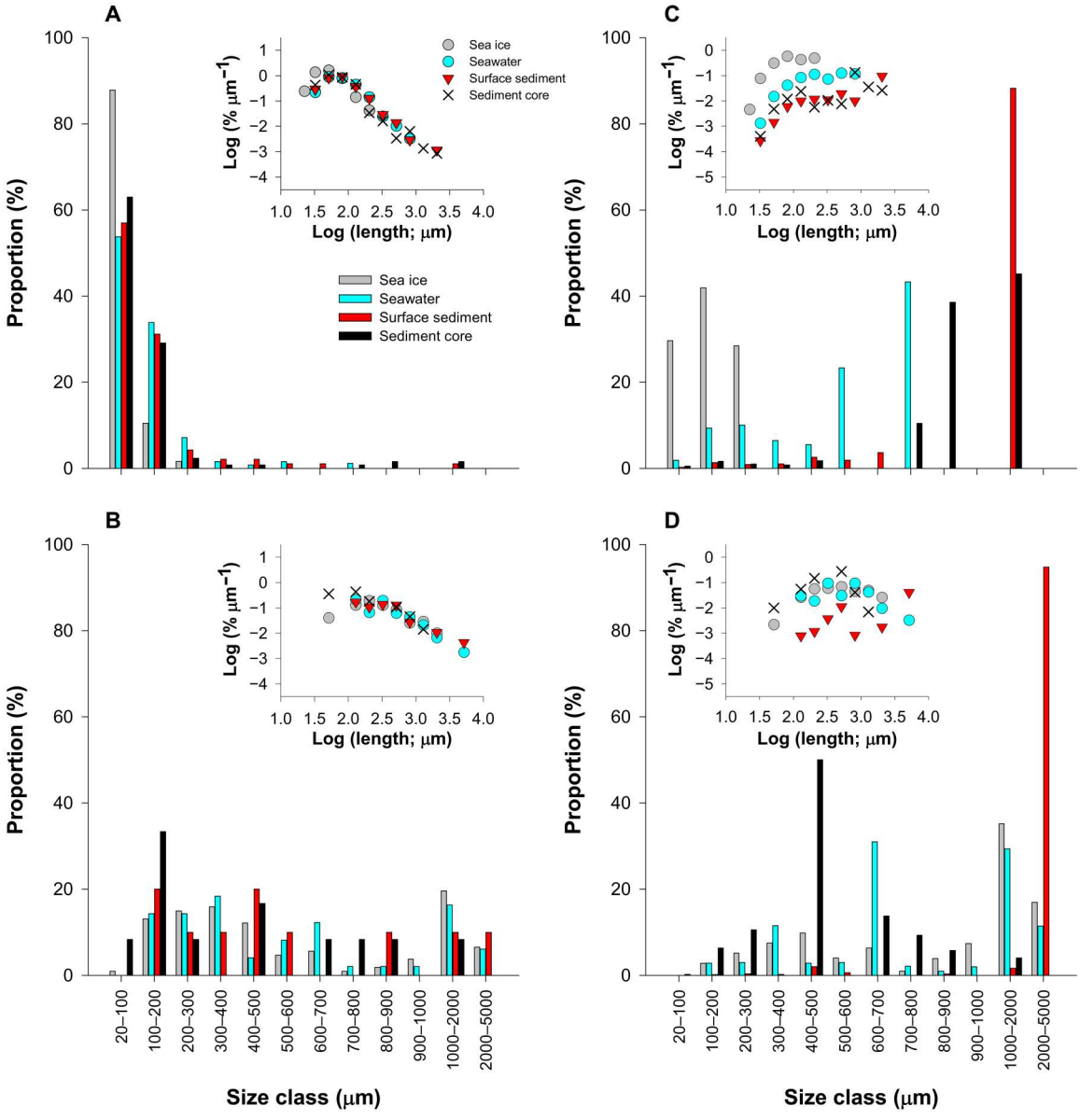


**Fig. 4. Size distributions of overall microplastic (MP) particles found in each compartment of the western Arctic Ocean (WAO).** (**A**) Number-based nonfibers. (**B**) Number-based fibers. (**C**) Mass-based nonfibers. (**D**) Mass-based fibers. Data for WAO sea ice were quoted from Kim *et al.* (*26*). Size distribution was obtained from a total of 1134 MP particles, consisting of 592 from sea ice, 300 from seawater, 103 from surface sediment, and 139 from sediment core. Inset images in each figure panel indicate the size distribution normalized by the bin width of each size class, for which a logarithmic binning with a multiplier of 1.58 (i.e., a constant logarithmic interval width of 0.2 μm) was applied (*26*).

## Mass-based MPs in water and sediments

The mass concentrations of MPs were 0.002 to 0.097 (mean ± SE, 0.024 ± 0.018) mg $m^{-3}$ for seawater, 0.18 to 34.5 (6.72 ± 5.57) mg $kg^{-1}$ for surface sediment, and 0.02 to 42.9 (6.87 ± 4.27) mg $kg^{-1}$ for sediment cores. The frequency of mass-based MPs tended to increase with increasing size, showing a contrast with the size distribution of the number-based MPs (Fig. 4, C and D) and consistent with those previously observed in other studies (*5*, *26*, *35*). The mass of nonfiber MPs accounted for >95% of the total mass in each of the three sample types, and this contribution did not substantially change with MP detection cutoff sizes because most of the total MP mass in a sample originated from large-sized nonfibers (fig. S7, A to C). For instance, although nonfibers larger than 200 μm were few in number (10% of MPs in seawater, 11% of MPs in surface sediments, and 7.2% of MPs in sediment cores), they constituted 86, 94, and 97% of the total mass of MPs, respectively. Consequently, the total MP mass in a sample was primarily determined by the presence of large-sized nonfiber polymers. Similarly, the polymer compositions in MP mass were less dependent on the MP cutoff size (fig. S7, D to F). The mass burial rate of MPs in the sediment core was rejected from the exponential increase when all MP particles were considered ($P > 0.05$); this was due to

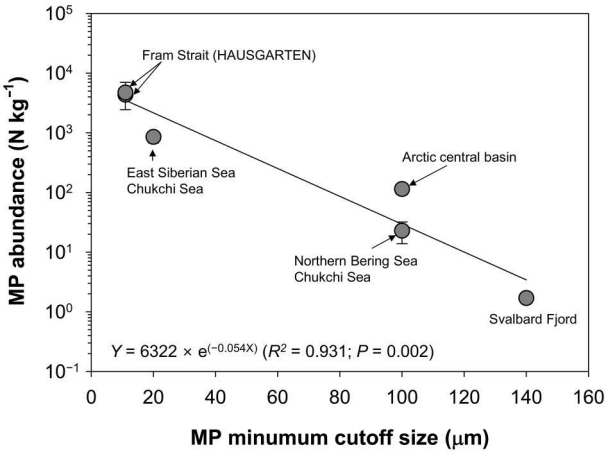


**Fig. 5. Dependence of microplastic (MP) abundance in Arctic surface sediment on measured MP detection cutoff size.** Data consist of three datasets from the Atlantic-side Arctic basin [4360 ± 675 N kg$^{-1}$ for MPs ≥11 μm (*27*) and 4730 ± 2284 N kg$^{-1}$ for MPs ≥11 μm (*30*) in the HAUSGRATEN stations; 1.7 ± 0.2 N kg$^{-1}$ for MPs ≥140 μm in Svalbard Fjord (*31*)], two datasets from the Pacific-side Arctic basin [22.9 ± 9.08 N kg$^{-1}$ for MPs ≥100 μm in the Northern Bering Sea/Chukchi Sea (*29*) and 854 ± 180 N kg$^{-1}$ for MPs ≥20 μm in size in East Siberian Sea/Chukchi Sea (this study)], and one dataset from the Arctic central basin [114 ± 22.5 N kg$^{-1}$ for MPs ≥100 μm in size (*28*)].

the variability in the presence of large-sized nonfiber polymers that were rare in number but substantially contributed to the total MP mass. The exclusion of nonfiber polymers >200 μm (9 of a total of 139 MP particles) produced a significant exponential fit with an increase rate similar to that of the number-based burial rate (Fig. 2D). Similar results were obtained for the estimates using a 20-year moving average without excluding nonfiber MPs >200 μm, showing significant correlations between the MP burial rates and plastic productions (fig. S8, A to C). The MP burial rate (0.0330 ± 0.0041 year$^{-1}$ for number-based; 0.0269 ± 0.0060 year$^{-1}$ for mass-based) was close to our estimates presented in Fig. 2 and produced similar WAO MP stocks in the post-1930 sediments (fig. S8, D and E).

When normalized by the width of the size-class interval, so that MP frequency was independent of the bin width, the size distributions showed peak frequencies (i.e., modes) in specific size classes. Below that, smaller MPs were more deficient than those expected from a power-law distribution (insets in Fig. 4, A and B), and resultant mass frequency decreased as the size decreased (insets in Fig. 4, C and D). This indicates that assuming a power-law distribution can lead to uncertainties (i.e., overestimation) particularly when number- and mass-based concentrations (and resultant MP stocks) of unmeasured small-sized MPs are estimated from the size distribution of measured larger MP particles.

## WAO MP loads

To compare MP stocks between the multiple compartments in the same domain of WAO (see Materials and Methods), we compiled data of MPs (≥20 μm) that could be temporarily trapped in WAO sea ice investigated in 2017 (*26*). In terms of MP quantities per unit volume in each compartment (N m$^{-3}$ or mg m$^{-3}$), the sediments presented four to five orders of magnitude higher accumulation potentials than seawater and 10 times (in number) to 1000 times (in mass) higher accumulation potentials than sea ice (Table 1). This

**Table 1. Plastic budget in each compartment of the western Arctic Ocean (WAO).** The means ± SE of microplastic (MP) amounts in number and mass are shown separately for the WAO seasonal sea ice region (area, 1.95 × 10$^6$ km$^2$). For seawater, the distribution of MPs was assumed to be vertically uniform within the water depth of the mixed layer water depth (50 m) or the average water depth of WAO (150 m). The MP amount for sea ice [cited from (*26*)] indicates the annually trapped or released MPs in the seasonal ice zone of the WAO. The annual increase rates (0.0320 year$^{-1}$ for number and 0.0329 year$^{-1}$ for mass) of plastic burial obtained from the S12 sediment core were applied to estimate the amounts of MPs buried in the 10-cm-thick sediment throughout the entire WAO seafloor since the 1930s. The total MP load (in bold) refers to the total amount of plastic retained in all compartments of the WAO as the sum of the MP amounts in seawater (150 m depth), sea ice (1.5 m thick), and sediment (0.1 m thick) of WAO. The percentage is the ratio of the MP amount in each compartment to the total MP load. VC$_x$:VC$_{seawater}$ refers to the ratio of the MP quantity per unit volume of each compartment (VC$_x$; in N or mg m$^{-3}$) to that of seawater (VC$_{seawater}$). Values in parentheses refer to the median values. Density of sea ice [0.91 g cm$^{-3}$; (*26*)] was considered for its volume calculation.

| Compartment | Depth or thickness (m) (volume; km$^3$) | Number-based MPs | | | Mass-based MPs | | |
|---|---|---|---|---|---|---|---|
| | | VC$_x$:VC$_{seawater}$ | MP number stock (× 10$^{16}$ N) | Percentage (%) | VC$_x$:VC$_{seawater}$ | MP mass stock (× 10$^3$ ton) | Percentage (%) |
| Seawater | 50 (9.7 × 10$^4$) | 1 (1) | 0.25 ± 0.11 (0.12) | 1.6 (0.9) | 1 (1) | 2.30 ± 1.79 (0.77) | 1.1 (1.4) |
| | 150 (2.9 × 10$^5$) | 1 (1) | 0.74 ± 0.34 (0.35) | 4.7 (2.6) | 1 (1) | 6.91 ± 5.38 (2.31) | 3.3 (4.2) |
| Sea ice | 1.5 (2.7 × 10$^3$) | 1.6 × 10$^3$ (2.7 × 10$^3$) | 11.5 ± 2.12 (9.30) | 73.2 (70.6) | 1.9 × 10$^2$ (3.1 × 10$^2$) | 13.4 ± 3.16 (7.11) | 6.4 (13.0) |
| Surface sediment | 0.02 (3.9 × 10$^1$) | 1.6 × 10$^4$ (3.5 × 10$^4$) | 1.59 ± 0.37 (1.61) | 10.1 (12.2) | 9.6 × 10$^4$ (6.9 × 10$^4$) | 88.8 ± 65.9 (21.1) | 42.1 (38.6) |
| Post-1930 sediment | 0.1 (1.9 × 10$^2$) | 3.1 × 10$^4$ (3.8 × 10$^4$) | 3.47 ± 0.80 (3.52) | 22.1 (26.8) | 1.5 × 10$^5$ (2.3 × 10$^4$) | 191 ± 142 (45.3) | 90.4 (82.8) |
| **Total plastic load** | | | **15.7 ± 2.30 (13.2)** | **100 (100)** | | **212 ± 142 (54.9)** | **100 (100)** |

finding points to the efficiency of the Arctic seafloor for sequestering and accumulating plastics in its sediments. Extrapolating the calculated MP stocks for each compartment to the whole volume of each compartment of the WAO, we estimate that a total of 15.7 (± 2.30) × $10^{16}$ N and 0.21 (± 0.14) MT of MPs ≥20 μm may be present (Table 1). Of the total loads, 22% in number and 90% in mass may have been buried in the upper 10 cm of sediments accumulated since the 1930s. The top 2 cm of surface sediment harbors MPs of 1.59 (± 0.37) × $10^{16}$ N and 0.09 (± 0.07) MT, which account for 10 and 42% of the total MP load, respectively. Although MPs were assumed to be distributed evenly throughout the 150 m water depth, the water column retained only 3 to 5% of WAO MPs.

The stock of MPs sequestered in surface sediment was sevenfold lower in number but sevenfold higher in mass than that of ice-trapped MPs. This difference was because larger (thus heavier) nonfiber polymers were more abundant in sediments than in sea ice; their average sizes were 66 ± 1.65 μm (23 to 230 μm; $N$ = 485) in sea ice (*26*), 142 ± 21.3 μm (35 to 1808 μm; $N$ = 93) in surface sediment, 132 ± 20.0 μm (30 to 1985 μm; $N$ = 127) in the sediment core, and 126 ± 6.93 μm (34 to 773 μm; $N$ = 251) in seawater. The average size of nonfiber MPs was similar between surface sediment and the sediment core (Mann-Whitney test, $P$ = 0.157) but significantly larger in sediments than in sea ice (Kruskal-Wallis test, $P$ < 0.001). In contrast, there were no significant differences in the average size of fiber MPs in the sea ice, surface sediment, and sediment core (Kruskal-Wallis test, $P$ = 0.308). In particular, nonfiber polymers >200 μm, contributing a greater component of MP mass in sediments, were much rarer in sea ice, accounting for 1.4% by number and 17% by mass. This finding confirms that number-based data are inappropriate for the estimation and comparison of plastic loads, although they are more informative of risk assessment to plastic exposure.

## DISCUSSION

Compared to the knowledge on the horizontal relocation of ice-captured MPs by sea ice drifting (*24*–*26*), knowledge regarding the role of sea ice in the vertical redistribution of MPs is more limited and at an ad hoc level. The WAO seasonal sea ice entraps hundreds (in mass) to thousands (in number) of times more MPs per unit volume than seawater (Table 1). Despite the presence of such a temporary sink, which might retard the deposition of plastics, the Arctic sediments exhibited a much greater quantity of plastic per cubic meter (particularly for mass) than sea ice. This implies that MPs may efficiently deposit on the Arctic seabed and then be sequestered in its sediments. The temporarily ice-trapped MPs of ~$10^{17}$ pieces and ~0.01 MT could be released and redistributed in the WAO region as the ice melted in summer. During redistribution, ice floes that remain unmelted in summer may facilitate the vertical deposition of MPs in the vicinity of the ice barrier by accumulating the MPs carried by both meltwater and Pacific waters as well as by accelerating the formation of sinking algal-MP aggregates. Over the past several decades, the WAO sea ice has continued to retreat (*34*), and the amount of plastics entering the WAO, as inferred in Fig. 2, may have increased. Such a combination of sea ice retreat and increasing plastic input might have led to more plastic deposition in regions further north, following the receding ice barrier. This hypothesis was corroborated by the relatively elevated MP abundance in both seawater and surface sediment around the northern summertime ice borderline region, contrary to the expected depletion of MPs in the ice borderline region due to wider spreading and dilution as sea ice retreats further north. The sedimentary MP distribution appeared to be more clearly skewed to the north when MPs ≥100 μm in the present study were compared together with the results of a previous study for MPs ≥100 μm, which considered only southern summertime ice-free regions (Bering Strait to Chukchi Sea) (see Fig. 1A) (*29*). Our finding is also supported by a similar result observed in sediments at the HAUSGRATEN observation stations located at the geographically opposite end of the Arctic to the WAO, which also showed the highest MP quantities at northernmost sites affected by sea ice (*27*). The MPs in our surface water samples showed a tendency to decrease toward the north after entering the Arctic at a high level and then increase again in the ice borderline region. In the summer of 2017 (the same season as our sediment survey), Mu *et al.* (*38*) also found a slightly higher MP abundance in seawater at polynya around the ice borderline, which is located north of our S22 and S26 sediment sites, than in the southern ice-free regions (see Fig. 1B). Coagulation with algae-excreted sticky exopolymers makes MP particles such as PP and PE negatively buoyant, which accelerates their vertical downward transport (*18*). Deposition of MPs onto the sea floor could thus be further enhanced in the ice borderline region via coagulation in sinking (ice) algal aggregates, given that the region supports plentiful formation of ice-algal aggregates beneath the sea ice (*49*). This hypothesis is supported not only by the significant correlation between the chlorophyll a content in overlying surface water and small-sized MPs (<100 μm) in surface sediments but also by the high proportions of buoyant PP in the sediments from the ice-borderline regions relative to ice-free regions, although PP proportion in seawater was relatively uniform across all sites. Bergmann *et al.* (*27*) also found a positive correlation between sedimentary MP abundance and chlorophyll a content, with elevated MP levels at the northernmost sites in the marginal sea ice zone. The relatively low MP levels at two southwestern East Siberian sites (S23 and S24) at distances of 185 to 325 km from site S26, despite their location around the ice barrier, may be because they have been affected by the intrusion of waters polluted with low levels of MPs, such as the Siberian coastal current, in addition to low algal activity. Tenfold lower contents of MPs (average, 0.01 N $m^{-3}$) were found in the East Siberian coastal surface waters (*50*), although a smaller net mesh size (200 μm) was used to collect these MPs compared with those obtained from the Chukchi Sea (average, 0.23 N $m^{-3}$ for ≥330 μm) (*38*). These seawater results are broadly consistent with the spatial distribution of the sedimentary MPs observed in the present study.

The highest MP pollution levels in Arctic surface sediments to date have been reported at the HAUSGRATEN observation stations (*27*, *30*), which were among the highest recorded from global benthic sediments (*51*). However, it should be considered that an MP detection size limit smaller than those in other studies (11 μm) was applied for the HAUSGRATEN sediments, and more than 70% of the MP particles found in those sediments were below 25 μm (*27*, *30*). The strong dependency of MP quantity on the measured MP detection size limit (see Fig. 5) suggests that MP pollution levels should be compared within the same size ranges. Compared with available datasets for the HAUSGRATEN sediments [8 to 142 N $kg^{-1}$ for >100 μm (*30*) and 0.89 to 9.43 (mean ± SE, 4.11 ± 1.16) N $kg^{-1}$ for >500 μm (*27*)], the WAO

sediments investigated in the present study showed higher average MP pollution levels in the same size ranges: 415 ± 92.4 (142 to 751) N $kg^{-1}$ for >100 μm and 58.0 ± 23.7 (0 to 148) N $kg^{-1}$ for >500 μm. The WAO sediments also retained significantly higher MP particles ≥100 μm than the Arctic central basin sediments (114 ± 22.5 N $kg^{-1}$; *t* test, $P = 0.017$) (*28*). This finding was consistent with the interbasin comparison results for ice-trapped MPs in the same size range (*24*–*26*), indicating that the WAO could be a notable region for the accumulation of MPs in the Arctic Ocean.

Recently, Martin *et al.* (*10*) suggested that 170 (29 to 900) MT, accounting for ~88% of the plastics that have entered the ocean since 1950, might have accumulated in the form of MPs and mesoplastics in the post-1950 global ocean sediments, most of which (66%) would have been at the continental slope of 200 to 2000 m depths. Although those authors highlighted the possibility of underestimating the cumulative ocean input of plastics, their results lead to further questions regarding the plastic budget when considering the prevalence of macroplastic debris stranded/buried on global shorelines (*11*, *52*), the vertical oscillation of MPs in subsurface water column (*20*), and the slow generation of secondary MPs owing to a low plastic degradation rate (*11*, *19*). A global ocean surface mass balance budget model for positively buoyant macroplastics [66.5% of produced plastics; (*1*)], including the terms for emission, transport (debris circulation dynamics in coastal environments), and degradation of plastics, showed that 66.8% of the post-1950 cumulative marine input of the macroplastics might have remained stranded/settled/buried along the global shorelines, with 0.9% in offshore water, and 32.3% would have transformed into secondary MPs under the degradation rate of 3% $year^{-1}$ (equivalent to a half-life of 23.1 years) (*11*). The model simulation and field measurements resulted in an average estimate of 14.5% for the fraction of MP stock to macroplastic stock in the OSL (*6*, *19*, *35*). Recent observations of pelagic MPs have shown that a substantial fraction of MPs resides below the OSL to the bottom layers of the oceanic water column due to the vertical sinking and oscillation, regardless of whether it is in coastal waters (*53*) or open ocean waters including mid-latitude offshores (*54*, *55*), the Atlantic Ocean (*56*), and Arctic Ocean (*30*, *57*, *58*). There was no clear pattern for vertical distribution of MPs below the OSL because MPs distributed relatively evenly in the whole subsurface layer, or sometimes, the maximum levels were in the intermediate or abyssal layer. Measurements in the literature (a total of 90 water columns) showed a wide range of 0 to 6.7 for the proportion of MPs measured in each subsurface layer to those in the uppermost water layer (fig. S9), implying that substantial quantities of MPs may remain in the global water column below the OSL without complete settlement into sediments. To understand the contribution of the WAO MP stock in global budget, we estimated the global ocean MP inventory by using a simplified mass balance model and current knowledge on the plastic budget, including the ocean input of plastics that are divided according to their size (primary MPs and macroplastics), origin (inland and ocean), and buoyancy (buoyant and nonbuoyant) (see the Supplementary Materials for details) (*1*, *4*, *13*). We estimate 267 (124 to 416) MT for the post-1950 cumulative plastic input, and that 70.3% of the total plastic stock in the global ocean may be present in the form of macroplastics (referring to all plastics >5 mm) and 29.7% [79.4 (38.5 to 126) MT] in the form of MPs (fig. S10). Koelmans *et al.* (*19*) estimated that 99.8% (~196 MT) of the plastics that had entered the ocean since 1950 had settled below the OSL by 2016. If the "directly settled non-buoyant macroplastics" that was included in their total plastic ocean stock is excluded, the MP stock is estimated at ~127 MT. It is necessary to notice that in their analytical mass balance model, all initially buoyant macroplastics entering the ocean were assumed to float always with none of them being stranded/settled/buried and to be transformed to secondary MPs over time during floating. In a global ocean surface mass balance budget model that included the modules for degradation of buoyant macroplastics as well as for their stranding, settling, and burial on shorelines, Lebreton *et al.* (*11*) estimated 41.9 (22.6 to 62.1) MT for the global marine MP stock. Our estimate for the global ocean MP stock corresponds to 63% of the estimate by Koelmans *et al.* (*19*) and approximately twice that of Lebreton *et al.* (*11*). Extrapolating the floating MP stock observed in the WAO to global ocean volume ($1.34 \times 10^9$ $km^3$), we can obtain 93.0 ± 28.5 MT for MPs in global ocean waters. In addition, the extrapolation of the WAO sedimentary MP stock to global seafloor area ($0.36 \times 10^9$ $km^2$) yields 35.6 ± 26.4 MT for the global sedimentary MP stock. The resultant total global ocean MP stock (~129 MT) extrapolated from the WAO MP stock exceeded our model estimate (79.4 MT), implying that the WAO MP stock might be above the global average of the ocean MP stock at the present time. This result is unexpected given that the Arctic is a pristine remote region far from mid-latitude regions where much of the plastic debris is emitted from, again implying the importance of WAO sediments in the remote region as sinks for MPs missing in the global ocean MP budget. The MP stock stored in WAO sediments can be also compared with those in ocean sediments near the plastic emission sources in mid-latitude regions. Martin *et al.* (*59*) estimated the post-1930 MP burial quantities in the Red Sea (340 ± 200 kg $km^{-2}$) and Arabian Gulf (660 ± 200 kg $km^{-2}$) mangrove sediments. The area-normalized MP stock accumulated in the WAO sediments since the 1930s was 98 ± 73 kg $km^{-2}$, which is at the 15 to 29% level of the MP stocks in mid-latitude mangrove sediments. However, owing to WAO's more than 6000 times wider area, the MP stock accumulated in WAO sediments since the 1930s is more than 1000 times greater than the post-1930 burial amounts of MPs (~160 tons) in the Red Sea and Arabian Gulf mangrove sediments.

Such high plastic accumulation in the WAO may be associated with its geophysical features. The clockwise Beaufort Gyre, the vortex activity of which has intensified over the past few decades (*60*), inhibits the introduced pollutants from leaving, and due to the increased residence time (*61*), the pollutants may accumulate in the regions affected by it. Specifically, the anticyclonic ice drift amplified during the late 2000s increased ice export into the study region at the southern boundary of the gyre (*62*). In a previous study, we found that some of the ice floes in the study region had been transported from the Beaufort Sea, and they contained more ice-trapped MPs than those from the East Siberian Sea (*26*). Such positive drivers associated with the Beaufort Gyre may have generated a high accumulation of environmentally nondegradable and nonvolatile pollutants such as plastic in the WAO region. The entry of highly MP-polluted North Pacific seawater (*63*) could be another driving force for MP accumulation in the WAO. A gradual increase with time in the MP pollution level has been observed in seawater of the northeast Pacific linked to a global hotspot of plastic discharge (i.e., the Asian continent and its marginal seas) (*35*, *63*). The Arctic influx of Pacific water through the Bering Strait has also increased ~50% in recent years due to oceanic warming and

the change in pressure head and wind (*64*). As expected, a multidecadal increase in MP burial was found in the WAO sediment core, supporting the proposition that the input of plastic to the WAO may have increased.

Given the high percentage of nonfibrous plastics in plastic resins produced worldwide (88 to 94%; w/w) (*1*, *65*), the dominant occurrence of fibrous polymers in other sediment samples worldwide (*51*) has long been questionable. Our notable finding is that MP composition in terms of polymer and shape could vary according to the measured cutoff sizes. In the present study with a size detection limit of 20 μm, nonfiber polymers (median size, 90 μm; $N$ = 471) were much more abundant in the small size ranges, but fibers (median size, 423 μm; $N$ = 71) dominated in the large size ranges. Similarly, more than 70% of the nonfiber MPs in the HAUSGRATEN surface sediments were present below 25 μm (*27*, *30*), while microfibers in the global dataset for oceanic waters had a larger size (median, 1.07 mm; $N$ = 2016) (*66*). Hence, a greater proportion of fibers than nonfibers may be found in the samples for which a large MP size was applied as its detection limit. This result suggests that the fiber dominance observed in previous coastal (*51*, *67*) and Arctic sediment studies (*28*, *29*, *31*) could be ascribed to their larger detection cutoff sizes of 100 to 500 μm. In contrast, nonfiber MPs accounted for 84 to 91% of the MPs (≥95% in mass) in seawater and sediments in our study, for which a smaller size detection limit (20 μm) was applied; these compositions are in excellent agreement with those in world plastic production. A similar issue related to size dependency can also be raised in terms of polymer composition that can be used to identify the source of MP particles. PE (including chlorinated and oxidized PE), one of the largest produced plastic resins, was not detected in the Arctic sediment samples with an MP size detection limit of 100 μm (*28*, *29*) but was found frequently with proportions of 17 and >30% in overall MP numbers, respectively, regardless of the location of the basin, when the cutoff size was lowered to 20 μm for WAO sediments (this study) and 11 μm for HAUSGRATEN sediments (*27*, *30*). Note that our WAO sediments harbored 71% of the overall PE particles in the <100-μm size class. This suggests the necessity of harmonizing MP size to avoid false conclusions potentially caused by comparing different MP data.

The high nonfiber-to-fiber ratio together with an exponential increase in MP burial observed in the present study suggests that the WAO sediments can provide an archive enabling us to trace historical plastic usage on the planet. The mass production of plastic at an 8.4% annual increase (*1*), coupled with inefficient waste management systems, is projected to further increase loads of plastic entering the ocean for the next several decades (*63*), and thus, plastic entering the Arctic will increase proportionally. Compared with the growth rate in plastic production, MP deposition to the Arctic seafloor occurred much more slowly, with an increase of ca. 3% $year^{-1}$ and a doubling time of 23 years. Brandon *et al.* (*67*) reported a 4.75% annual increase rate (a doubling time of 15 years) for MP deposition in the coastal sediment of the Santa Barbara basin, California. This indicates a possible lag time between plastic production and MP deposition on the ocean seafloor, with a longer lag time for Arctic deposition in particular. Considering these lag times, which means the retardation in the delivery and deposition of plastic to the Arctic, the plastic pollution level in the Arctic environment will not reach its peak for many years, even after production and ocean input are drastically reduced or even completely ceased. A recalculated longer residence time of plastic in the ocean surface may predict this unfortunate future (*15*). Using the Globo-POP model, Wania (*68*) predicted that nondegradable and nonvolatile pollutants delivered from the mid-latitudes via ocean currents would continuously increase in Arctic waters and peak after 25 years, even if the emissions were zero or notably reduced. Therefore, globally concerted vigorous action to substantially reduce the plastic ocean input is urgently needed to protect the Arctic environment. The recent resolution of the United Nations Environment Assembly to end plastic pollution and forge an international legally binding agreement by the end of 2024 could be the historic first step necessary for the sustainability of our planet (*2*, *3*).

Here, we showed that Arctic sediments can act as important current and future sinks of MPs. We did not include macro- and mega-sized plastic debris (more than several centimeters in size), and we considered only the WAO region, equivalent to 13% of the Arctic Ocean area. The macro- and mega-sized plastic debris found on the Arctic sea floor have also increased over the past decades (*69*, *70*). In this respect, the contribution of plastics stored on the Arctic seabed to the global plastic budget may be greater than our estimates for MPs. Specifically, the WAO region is undergoing rapid changes in the aforementioned geophysical conditions. In addition, anomalously high surface phytoplankton blooms were found around the WAO sea ice borderline, which were associated with an unprecedented supply of nutrients caused by the intrusion of Atlantic-origin cold saline water (*48*). Interannual changes in biological and geophysical conditions, which are strongly associated with sea ice decline and can be reinforced by climate change (*47*), may affect the amount and distribution of plastic deposited to the Arctic sea floor. Our results suggest that not only the deposition of plastic to the Arctic seabed may be enhanced by sea ice but also, when considering continued sea ice retreat and increasing plastic input, the plastic accumulation zone may extend further northward in the future. High MP accumulation in sediments can affect benthic organisms, including causing changes in communities (*71*). Future studies, including long-term monitoring in wider areas and sediment coring in northern sites, are warranted to establish the mechanistic links between plastic accumulation and sea ice in greater detail and to identify the adverse effects on benthic organisms caused by high MP accumulation in the Arctic environment.

## MATERIALS AND METHODS

### Study area

The study area covered the Bering, East Siberian, and Chukchi Seas of the WAO, with a special focus on the region where sea ice repeatedly forms and melts yearly: 150°E (East Siberian Sea) to 120°W (Beaufort Sea) longitude and 66°34′N (Bering Strait) to the 10-year mean September retreat line latitude (*26*). The sea ice extent in the WAO extends to the south of the Bering Sea in winter and retreats to the north of the Chukchi Sea and the East Siberian Sea in summer. The summer sea ice extent in this region has continuously retreated over the past few decades (Fig. 1A). Pacific water of 0.83 Sv (1 Sv = $10^6$ $m^3$ $s^{-1}$) enters the WAO annually through the Bering Strait (*72*), and the influx has increased to more than 1 Sv in recent years (*64*). Pacific warm water flows to the north but mostly along the east coast of the Canadian basin, resulting in the summer sea ice retreat line skewing toward the East Siberian Sea. Ice floes

around the summer retreat line, some of which originate from the Beaufort Sea and others from the East Siberian Sea, have paths drifting along the southern boundary of the clockwise Beaufort Gyre (*26*).

### Sediment sampling

Sediment samples were collected from the continental shelf and slope of the WAO basin (water depth, 51 to 529 m) in August 2017 during the Korean IBRV *Araon* expedition (ARA08B). The sampling sites consisted of two regions: the northern parts of the Chukchi (S12 and S14; 72°21.6′N to 73°34.8′N) and East Siberian Seas (S22 to S24, and S26; 74°00.0′N to 75°46.2′N) (Fig. 1A and table S1). The sites in the Chukchi Sea had no sea ice coverage in summer, whereas the sampling sites in the East Siberian Sea were located around the summer retreat line of the 2017 sea ice extent. The two sampling regions also represented the ice-free and ice borderline regions in the summers of the 2010s (see the ice retreat lines in Fig. 1A). Two surface sediment samples from the Chukchi basin were collected from the continental shelf (S12) and slope (S14), which were located on the main route of the northern flux of inflowing Pacific seawater. Four surface sediment samples from the East Siberian basin were taken from the continental shelf (S24) and slope (S22, S23, and S26), which encounters the southern boundary flow of the clockwise Beaufort Gyre as well as a branch of the Pacific inflow (*73*). In addition, one 35-cm-thick sediment core sample (ARA08B/12) was collected separately from the surface sediment at the S12 site.

All sediment samples were collected using a stainless steel box corer (40 cm × 30 cm × 60 cm). After the box corer was retrieved, the top 2 cm of surface sediments was collected using a precleaned stainless steel spoon and kept frozen in a precleaned glass jar before analysis. A subcore sample was taken using a cylindrical polycarbonate (PC) core liner (60 cm in length and 10 cm in diameter) to assess the vertical profile of MPs in the sediment taken from site S12. The top and bottom of the subcore sample were sealed with a polystyrene (PS) lid and kept at 4°C before analysis. In the laboratory, the core sample was vertically divided into two half sides. Samples from one half-side were used to determine environmental variables [i.e., water content, dry bulk density (DBD), and TOC] and sediment chronology, while samples from the other half-side samples were used to determine MPs and dinoflagellate cysts. An aliquot of each subsample for environmental variables was taken from each layer at 1-cm intervals. Each sample was weighed and dried at 105°C until reaching a constant weight, and the water content was determined using the weight loss after drying. The dried samples were used to determine DBD, TOC, and $^{210}$Pb activities. Grain density was measured using a He pycnometer (AccPyc 1340, Micromeritics Instrument Corp., USA), and DBD (g cm$^{-3}$) was calculated from the measured water contents and grain density. The TOC content was obtained by measuring the difference between the total carbon and total inorganic carbon content measured using a CHN elemental analyzer (FLASH 2000, Thermo Fisher Scientific). The chlorophyll a content was determined for seawater taken from the five water depths, 1, 10, 20, 30, and 40 m (or 50 m), at each sediment sampling site. Chlorophyll a was measured onboard using a fluorometer (Trilogy, Turner Designs, USA) after extraction with 90% acetone for 24 hours from the samples immediately filtered through a glass fiber filter (47 mm; Whatman GF/F). The average value of chlorophyll a content at five water depths was used to test the relationship with sedimentary MP abundance.

For MP analysis, sediments from the subcore were sliced with transversely at 1-cm intervals, collected using a precleaned stainless steel spoon, and stored frozen in a precleaned glass jar before further processing. To rule out potential MP contamination that might have occurred during core cutting and sample collection, we removed a few millimeters from the surface that was exposed to the air, a PS lid, or a core liner before sample collection using a precleaned stainless steel spoon. The water content of each bottled sediment sample was again determined using an aliquot of the homogenized subsample (~2 g per sample) to correct any change in water content during the sample collection process, which was used to normalize the MP content to the value based on the dry weight of the sediment. The entire sample remaining in each bottle (4.39 to 13.88 g dry weight) was used to analyze MPs. The water content of surface sediment samples was determined from an aliquot of the homogenized subsample (~5 g per sample). The surface sediment of 19.7 to 21.1 g (dry weight) was used for MP analysis.

### Seawater sampling

Seawater samples were collected during the *Araon* expedition (ARA10B) in August 2019. Near-surface seawater samples (6 to 7 m depth) were collected from five locations, covering ice-free regions from the south (W1; 69°10.7′N) to the north (W2 to W4; 74°48.0′N to 76°21.1′N) of the Chukchi Sea and the ice borderline region (W5; 79°36.9′N) (table S2 and Fig. 1B). Approximately 1.7 to 5.3 m$^3$ of seawater were collected at each location with stainless steel piping, which was partly composed of polyvinyl chloride (PVC), for 5 hours at a flow rate of 5 to 16 liters min$^{-1}$ while the vessel navigated. Seawater samples were directly filtered through a net with a mesh size of 20 μm, and the volume-reduced sample was then further filtered through a stainless steel filter (pore size of 20 μm) in the laboratory. This sampling method has advantages over trawling a manta or neuston net (normally a mesh size of >300 μm), as it allows not only continuous collection of water in a wider section (~100 km per sample) without being disturbed by drifting ice pieces but also collection of small-sized MP particles (20 μm in this study) (*58*).

### MP analysis

Details of the MP analysis procedure are provided in Supplementary Text and fig. S11. MPs were separated from the sediment (13.8 to 50 g wet weight) using a modified protocol of the National Oceanic and Atmospheric Administration laboratory method (*74*). The protocol consists of successive steps of stirring and density separation in a solution of $ZnCl_2$:$CaCl_2$ (specific density, ~1.58 g cm$^{-3}$), filtration of the supernatant, additional density separation of filtered particles, digestion of organic materials in KOH and $H_2O_2$ solution, and a final filtration to isolate MPs from interfering particles. For seawater, the digestion of organic matter and density separation were successively conducted to isolate the MPs from filtered particles. The MP particles were identified using a μ-FTIR microscope (LUMOS, Bruker) following the method presented in a previous study (*26*). The spectra of all potential particles ≥20 μm in size in each filter were individually recorded in transmission mode to avoid human error caused by the preselection of "MP-like particles." The geometric shapes of the particles identified as synthetic plastic

polymers were classified into four types (fragments, fibers, sheets, and spherules) according to the same classification criteria as previous studies (*26*, *37*), and their longest dimension was measured and recorded as their size. The thickness of the fiber MPs was also measured. In this study, acrylic fibers were assigned to PAN according to a previous classification (*75*), while rayon was not included owing to its similarity to natural polymers with regard to the FTIR spectra (*26*).

### Contamination prevention and method validation

Strict control protocols were followed to prevent potential contamination during the entire sample treatment and analysis (Supplementary Text). Although laboratory ware made of glass or stainless steel was used after thorough rinsing with MP-free water, some polymer-based items were used for sample collection (PVC for seawater samples and PC and PS for sediment core samples) or treatment [polytetrafluoroethylene (PTFE) bottles containing MP-free water used for laboratory ware rinsing]. To completely rule out all potential contamination effects, we excluded all plastic particles that could have originated from the polymer-based items used during sample processing: PTFE from all samples, PVC from water samples, and PS and PC from sediment core samples. The excluded polymers were not notable MP components in the western Arctic samples (*26*, *29*, *38*, *58*). Potential contamination was further monitored using procedural blank samples ($N = 1$ for water, $N = 1$ for surface sediment, and $N = 2$ for sediment core) that were analyzed together with the samples in the same batch. MP particles of zero to three pieces were found in the blanks, and thus, the amount of MP in each sample of a batch was corrected by subtracting the amount of MPs found in the procedural blanks of the same batch. To validate the analytical methods, we also assessed the recovery and reproducibility of MPs by analyzing MP particles with different polymers, shapes, and sizes that were spiked into MP-free water and sediment samples (see details in Supplementary Text). Triplicate analysis for each mixture of sediment and water showed acceptable recovery ranges of 72.5 to 97.0% on average with a relative SD of 2.7 to 27.0% for the spiked nonfibers and fibers (tables S3 and S4).

### Sediment core dating and MP burial rate

$^{210}$Pb activities were analyzed for sediment chronology (i.e., age dating) for 11 layers of the entire core: 0 to 1 cm, 1 to 2 cm, 2 to 3 cm, 4 to 5 cm, 6 to 7 cm, 9 to 10 cm, 14 to 15 cm, 19 to 20 cm, 29 to 30 cm, 34 to 35 cm, and 35 to 36 cm. The sediment chronology of core ARA08B/12 was based on $^{210}$Pb measurements. The $^{210}$Pb activities were measured using a silicon surface barrier alpha spectrometer (Canberra Inc., PIPS) at the Korea Basic Science Institute. The excess $^{210}$Pb ($^{210}Pb_{ex}$) was calculated by subtracting the activity supported by its parent isotope, $^{226}$Ra, from the total $^{210}$Pb activity ($^{210}Pb_{total}$) in the sediment. The $^{210}Pb_{total}$ activities ranged from 14 to 53 mBq $g^{-1}$ of dry sediment weight, and the depth profiles of $^{210}Pb_{total}$ and $^{210}Pb_{ex}$ showed a typical $^{210}$Pb profile observed in the WAO (Fig. 2A) (*41*, *42*, *76*). The sediment accumulation rate (cm $year^{-1}$) was determined from the slope of the linear regression line of best fit on a logarithmic scale of $^{210}Pb_{ex}$ activity versus depth using the constant flux–constant sedimentation model, which assumes a steady state accumulation of sediments and that $^{210}Pb_{ex}$ activity of depositing sediment particles is constant (*40*). The $^{210}Pb_{ex}$ activities decreased exponentially below the SML, resulting in an estimated linear sedimentation rate (LAR) of 0.107 cm $year^{-1}$ for the S12 sediment core. This LAR value was well consistent with that of Kim *et al.* (*77*) at 0.09 cm $year^{-1}$ of $^{210}$Pb-derived LAR in a site (73.52°N, 168.94°W, 72.5 m water depth) approximately 22 km away from S12. The LAR for the S12 sediment core was also within a similar range as those reported from other sites of the WAO (average ± SE = 0.141 ± 0.032 cm $year^{-1}$; $N = 22$ sediment core samples), including the Bering Slope and the shelf area of the Chukchi Sea and the East Siberian Sea (0.17 ± 0.05 cm $year^{-1}$; $N = 15$) (*41*), the northern Chukchi Sea shelf (0.094 ± 0.019 cm $year^{-1}$; $N = 5$) (*42*), and the Chukchi Sea slope (0.06 cm $year^{-1}$; $N = 1$) (*76*), all of which were based on $^{210}$Pb measurements. Therefore, applying the LAR of the S12 sediment core (0.107 cm $year^{-1}$) to the entire WAO area does not cause substantial errors in the estimated MP amount sequestered in sediments accumulated in the WAO since the 1930s.

MP analysis focused on layers dated after the 1930s, the onset of industrial plastic production (*43*). Thus, the top 10 layers of the core (0 to 10 cm) dated from 1933 to 2012 were processed. The burial rates of MP (in number or milligrams of MP per square meter per year) were calculated as the product of DBD of the sediment, the MP quantity per gram of dry weight of the sediment, and the LAR. Only a few nonfiber polymer items larger than 200 μm in size (9 of a total of 139 polymer particles found in the entire sediment core) were found in some layers (three in the 0- to 1-cm layer, three in the 2- to 3-cm layer, two in the 5- to 6-cm layer, and one in the 7- to 8-cm layer); however, they accounted for >91% of the total MP mass in each of the four layers. When calculating the MP mass burial rate, the large-sized nonfiber polymers (>200 μm) were excluded because they caused bias in the total MP mass compared with the total MP number in the layer that they occurred in (Supplementary Text and fig. S12). To validate our results, we conducted additional analysis using a 20-year moving average of burial rates without excluding nonfiber MPs >200 μm based on the method discussed by Martin *et al.* (*59*) (fig. S8).

### Mass estimation of MP particles

Mass-based data were obtained by estimating the weights of individual polymer particles using the same method proposed for ice-trapped MPs (*26*) because it is difficult to weigh micrometer-sized objects in practice. This method infers the weight as the product of volume [estimated from observed morphological features such as four geometric shape types, the measured length of the longest cross section, and the estimated (or measured) thickness] and density (obtained from the FTIR characterization of polymers). For the same reason, similar attempts have been made to estimate the weights of MP particles based on the morphological features of particles (*5*, *59*, *78*) or number-to-mass conversion factors (*15*). Our method produced 10-fold higher mass values (for fragment-type MPs) than the estimates obtained by a similar geometric morphology-based model assuming an ellipsoid (*78*) but one to two orders of magnitude smaller than the estimates obtained using conversion factors (*15*). The MP mass yielded by our method was evaluated to be within one order range of those quantified using gas chromatographic mass spectrometry coupled with pyrolysis (*26*).

### Budgeting for MPs in Arctic compartments

We conducted budgeting for MPs retained in sea ice, seawater, and sediment to obtain the total MP load in the WAO. The amount of MPs trapped in (or released from) sea ice was estimated in a

previous study for the seasonal sea ice region of the WAO (*26*). For comparison with the ice-trapped ones, total MP amounts (*N* in number or tons in mass) in seawater and sediment of the same region (area of $1.95 \times 10^6$ km$^2$; no consideration of seafloor slope and roughness) were calculated by extrapolating the MP number or mass stocks in 1-m$^3$ volume of each compartment observed in the present study to the whole volume of each compartment in the WAO study domain. The top 2 cm of the surface was considered when estimating the MP load in the surface sediment. To estimate the MP amounts sequestered in sediments accumulated in the whole area of the WAO since the 1930s, we assumed that the LAR and the annual rate of increase in MP burial at all six sites of the WAO were the same as those observed at S12 since a similar average LAR was observed across the entire WAO basin, but relevant MP burial rate data for the WAO have not been reported so far. We first estimated the MP amounts buried in the upper 10 cm of sediments at each site (i.e., post-1930 cumulative MP amount) using the MP quantity in the top 2 cm of sediment at each site and the annual increase rates (0.0320 year$^{-1}$ for MP number and 0.0329 year$^{-1}$ for MP mass) of exponential curves obtained from the S12 sediment core and then extrapolated the values to the whole WAO area (Supplementary Text, table S5, and fig. S13). The MP budget in the water column was calculated for the polar mixed layer (50 m) of the WAO (*48*), assuming that the MPs were well mixed in the layer. Additional seawater MP budgeting was conducted for the average water depth of the WAO study domain (ca. 150 m) by conservatively assuming that MPs evenly distribute throughout the water column, given that MP abundances in Arctic deep and bottom waters were not substantially reduced compared with those in polar mixed layer (*57*, *58*).

### Data treatment and statistical analysis

Four geometric shapes were further grouped into nonfiber (a sum of fragments, sheets, and spherules) and fiber because the two geometry groups had different size distributions and fragmentation mechanisms (*26*). In this study, the term "MPs" or "total MPs" indicates the sum of all MP particles in size, polymer, or shape unless otherwise notified. MP abundance (in N kg$^{-1}$) and mass concentration (in mg kg$^{-1}$) for sediments were presented on the basis of the dry weight of sediment and then were converted to MP quantity per cubic meter of sediment using DBD of sediment to compare with plastic stocks in the same volume of seawater and sea ice. The relationships between MP abundance and environmental variables (water content, porosity, TOC, chlorophyll a content, and water depth) were tested using Pearson's correlation. The relationships between MP deposition and world plastic production in Fig. 2B were tested using a nonparametric test, Spearman's rank correlation, since the data were not normally distributed (Shapiro-Wilk normality test; $W = 0.842$ and $P = 0.047$ for nonfibers; $W = 0.734$ and $P = 0.02$ for fibers). Owing to the same reason, the relationships in figs. S4 and S8 were tested by Spearman's rank correlation. The difference in average sizes of MPs was tested using the Mann-Whitney test for between two groups and Kruskal-Wallis test for between three groups because of nonnormality in their distribution (Shapiro-Wilk normality test; $P < 0.001$ for all compared groups). For MPs in the S12 sediment core, the exponential growth curve was fitted to a simple exponent with two parameters to test the hypothesis of exponential increases in burial rates and quantities of plastic and to obtain the annual rates of increase for plastic deposition. All statistical analyses were performed in SPSS Statistics version 25. All values are reported as means ± SE.

## Supplementary Materials

**This PDF file includes:**

Supplementary Text
Figs. S1 to S13
Tables S1 to S5
Legends for data S1 to S5
References

**Other Supplementary Material for this manuscript includes the following:**

Data S1 to S5

## REFERENCES AND NOTES


1. R. Geyer, J. R. Jambeck, K. L. Law, Production, use, and fate of all plastics ever made. *Sci. Adv.* **3**, e1700782 (2017).
2. United Nations Environment Programme (UNEP), 2022; https://unep.org/news-and-stories/story/what-you-need-know-about-plastic-pollution-resolution.
3. United Nations Environment Programme (UNEP); 2021. https://unep.org/resources/pollution-solution-global-assessment-marine-litter-and-plastic-pollution.
4. J. R. Jambeck, R. Geyer, C. Wilcox, T. R. Siegler, M. Perryman, A. Andrady, R. Narayan, K. L. Law, Plastic waste inputs from land into the ocean. *Science* **347**, 768–771 (2015).
5. A. Cózar, F. Echevarría, J. I. González-Gordillo, X. Irigoien, B. Úbeda, S. Hernández-León, Á. T. Palma, S. Navarro, J. García-de-Lomas, A. Ruiz, M. L. Fernández-de-Puelles, C. M. Duarte, Plastic debris in the open ocean. *Proc. Natl. Acad. Sci. U.S.A.* **111**, 10239–10244 (2014).
6. M. Eriksen, L. C. M. Lebreton, H. S. Carson, M. Thiel, C. J. Moore, J. C. Borerro, F. Galgani, P. G. Ryan, J. Reisser, Plastic pollution in the world's oceans: More than 5 trillion plastic pieces weighing over 250,000 tons afloat at sea. *PLOS ONE* **9**, e111913 (2014).
7. E. van Sebille, C. Wilcox, L. Lebreton, N. Maximenko, B. D. Hardesty, J. A. van Franeker, M. Eriksen, D. Siegel, F. Galgani, K. L. Law, A global inventory of small floating plastic debris. *Environ. Res. Lett.* **10**, 124006 (2015).
8. L. C. Woodall, A. Sanchez-Vidal, M. Canals, G. L. Paterson, R. Coppock, V. Sleight, A. Calafat, A. D. Rogers, B. E. Narayanaswamy, R. C. Thompson, The deep sea is a major sink for microplastic debris. *R. Soc. Open Sci.* **1**, 140317 (2014).
9. F. Pohl, J. T. Eggenhuisen, I. A. Kane, M. A. Clare, Transport and burial of microplastics in deep-marine sediments by turbidity currents. *Environ. Sci. Technol.* **54**, 4180–4189 (2020).
10. C. Martin, C. A. Young, L. Valluzzi, C. M. Duarte, Ocean sediments as the global sink for marine micro- and mesoplastics. *Limnol. Oceanogr. Lett.* **7**, 235–243 (2022).
11. L. Lebreton, M. Egger, B. Slat, A global mass budget for positively buoyant macroplastic debris in the ocean. *Sci. Rep.* **9**, 12922 (2019).
12. L. C. M. Lebreton, J. van der Zwet, J.-W. Damsteeg, B. Slat, A. Andrady, J. Reisser, River plastic emissions to the world's oceans. *Nat. Commun.* **8**, 15611 (2017).
13. A. Forrest, L. Giacovazzi, S. Dunlop, J. Reisser, D. Tickler, A. Jamieson, J. J. Meeuwig, Eliminating plastic pollution: How a voluntary contribution from industry will drive the circular plastics economy. *Front. Mar. Sci.* **6**, 627 (2019).
14. L. J. J. Meijer, T. van Emmerik, R. van der Ent, C. Schmidt, L. Lebreton, More than 1000 rivers account for 80% of global riverine plastic emissions into the ocean. *Sci. Adv.* **7**, eaaz5803 (2021).
15. L. Weiss, W. Ludwig, S. Heussner, M. Canals, J.-F. Ghiglione, C. Estournel, M. Constant, P. Kerhervé, The missing ocean plastic sink: Gone with the rivers. *Science* **373**, 107–111 (2021).
16. D. Lobelle, M. Cunliffe, Early microbial biofilm formation on marine plastic debris. *Mar. Pollut. Bull.* **62**, 197–200 (2011).
17. M. Cole, P. Lindeque, E. Fileman, C. Halsband, R. Goodhead, J. Moger, T. S. Galloway, Microplastic ingestion by zooplankton. *Environ. Sci. Technol.* **47**, 6646–6655 (2013).
18. M. Long, B. Moriceau, M. Gallinari, C. Lambert, A. Huvet, J. Raffray, P. Soudant, Interactions between microplastics and phytoplankton aggregates: Impact on their respective fates. *Mar. Chem.* **175**, 39–46 (2015).
19. A. A. Koelmans, M. Kooi, K. L. Law, E. van Sebille, All is not lost: Deriving a top-down mass budget of plastic at sea. *Environ. Res. Lett.* **12**, 114028 (2017).
20. M. Kooi, E. H. van Nes, M. Scheffer, A. A. Koelmans, Ups and downs in the ocean: Effects of biofouling on vertical transport of microplastics. *Environ. Sci. Technol.* **51**, 7963–7971 (2017).

21. A. Cózar, E. Martí, C. M. Duarte, J. García-de-Lomas, E. van Sebille, T. J. Ballatore, V. M. Eguíluz, J. I. González-Gordillo, M. L. Pedrotti, F. Echevarría, R. Troublè, X. Irigoien, The Arctic Ocean as a dead end for floating plastics in the North Atlantic branch of the thermohaline circulation. *Sci. Adv.* **3**, e1600582 (2017).
22. N. Evangeliou, H. Grythe, Z. Klimont, C. Heyes, S. Eckhardt, S. Lopez-Aparicio, A. Stohl, Atmospheric transport is a major pathway of microplastics to remote regions. *Nat. Commun.* **11**, 3381 (2020).
23. C. L. Parkinson, N. E. DiGirolamo, Sea ice extents continue to set new records: Arctic, Antarctic, and global results. *Remote Sens. Environ.* **267**, 112753 (2021).
24. I. Peeken, S. Primpke, B. Beyer, J. Gütermann, C. Katlein, T. Krumpen, M. Bergmann, L. Hehemann, G. Gerdts, Arctic sea ice is an important temporal sink and means of transport for microplastic. *Nat. Commun.* **9**, 1505 (2018).
25. L. D. K. Kanhai, K. Gardfeldt, T. Krumpen, R. C. Thompson, I. O'Connor, Microplastics in sea ice and seawater beneath ice floes from the Arctic Ocean. *Sci. Rep.* **10**, 5004 (2020).
26. S.-K. Kim, H.-J. Lee, J.-S. Kim, S.-H. Kang, E.-J. Yang, K.-H. Cho, Z. Tian, A. Andrady, Importance of seasonal sea ice in the western Arctic Ocean to the Arctic and global microplastic budgets. *J. Hazard. Mater.* **418**, 125971 (2021).
27. M. Bergmann, V. Wirzbergeer, T. Krumpen, C. Lorenz, S. Primpke, M. B. Tekman, G. Gerdts, High quantities of microplastic in Arctic deep-sea sediments from the HAUSGARTEN observatory. *Environ. Sci. Technol.* **51**, 11000–11010 (2017).
28. L. D. K. Kanhai, C. Johansson, J. P. G. L. Frias, K. Gardfeldt, R. C. Thompson, I. O'Connor, Deep sea sediments of the Arctic Central Basin: A potential sink for microplastics. *Deep Sea Res. Part I Oceanogr. Res. Pap.* **145**, 137–142 (2019).
29. J. Mu, L. Qu, F. Jin, S. Zhang, C. Fang, X. Ma, W. Zhang, C. Huo, Y. Cong, J. Wang, Abundance and distribution of microplastics in the surface sediments from the northern Bering and Chukchi Seas. *Environ. Pollut.* **245**, 122–130 (2019).
30. M. B. Tekman, C. Wekerle, C. Lorenz, S. Primpke, C. Hasemann, G. Gerdt, M. Bergmann, Tying up loose ends of microplastic pollution in the Arctic: Distribution from the sea surface through the water column to deep-sea sediments at the HAUSGARTEN observatory. *Environ. Sci. Technol.* **54**, 4079–4090 (2020).
31. F. Collard, K. Husum, G. Eppe, C. Malherbe, I. G. Hallanger, D. V. Divine, G. W. Gabrielsen, Anthropogenic particles in sediment from an Arctic fjord. *Sci. Total Environ.* **772**, 145575 (2021).
32. M. Afenyo, B. Veitch, F. Khan, A state-of-the-art review of fate and transport of oil spills in open and ice-covered water. *Ocean Eng.* **119**, 233–248 (2016).
33. S. Kelly, E. Popova, Y. Aksenov, R. Marsh, A. Yool, Lagrangian modeling of Arctic Ocean circulation pathways: Impact of advection on spread of pollutants. *J. Geophys. Res. Oceans* **123**, 2882–2902 (2018).
34. J. Stroeve, D. Notz, Changing state of Arctic sea ice across all seasons. *Environ. Res. Lett.* **13**, 103001 (2018).
35. L. Lebreton, B. Slat, F. Ferrari, B. Sainte-Rose, J. Aitken, R. Marthouse, S. Hajbane, S. Cunsolo, A. Schwarz, A. Levivier, K. Noble, P. Debeljak, H. Maral, R. Schoeneich-Argent, R. Brambini, J. Reisser, Evidence that the Great Pacific Garbage Patch is rapidly accumulating plastic. *Sci. Rep.* **8**, 4666 (2018).
36. M. G. J. Löder, M. Kuczera, S. Mintenig, C. Lorenz, G. Gerdts, Focal plane array detector-based micro-fourier-transform infrared imaging for the analysis of microplastics in environmental samples. *Environ. Chem.* **12**, 563–581 (2015).
37. V. Hidalgo-Ruz, L. Gutow, R. C. Thompson, M. Thiel, Microplastics in the marine environment: A review of the methods used for identification and quantification. *Environ. Sci. Technol.* **46**, 3060–3075 (2012).
38. J. Mu, S. Zhang, L. Qu, F. Jin, C. Fang, X. Ma, W. Zhang, J. Wang, Microplastics abundance and characteristics in surface waters from the Northwest Pacific, the Bering Sea, and the Chukchi Sea. *Mar. Pollut. Bull.* **143**, 58–65 (2019).
39. D.-H. Chae, I.-S. Kim, S.-K. Kim, Y. K. Song, W. J. Shim, Abundance and distribution characteristics of microplastics in surface seawaters of the Incheon/Kyeonggi coastal region. *Arch. Environ. Contam. Toxicol.* **69**, 269–278 (2015).
40. A. Arias-Ortiz, P. Masqué, J. Garcia-Orellana, O. Serrano, I. Mazarrasa, N. Marbà, C. E. Lovelock, P. S. Lavery, C. M. Duarte, Reviews and syntheses: $^{210}$Pb-derived sediment and carbon accumulation rates in vegetated coastal ecosystems—Setting the record straight. *Biogeosciences* **15**, 6791–6818 (2018).
41. L. W. Cooper, J. M. Grebmeier, Deposition patterns on the Chukchi shelf using radionuclide inventories in relation to surface sediment characteristics. *Deep Sea Res. Part II Top. Stud. Oceanogr.* **152**, 48–66 (2018).
42. A. S. Astakhov, A. A. Bosin, Y. G. Liu, A. V. Darin, I. A. Kalugin, A. V. Artemova, V. V. Babich, M. S. Melgunov, Y. P. Vasilenko, E. G. Vologina, Reconstruction of ice conditions in the northern Chukchi Sea during recent centuries: Geochemical proxy compared with observed data. *Quat. Int.* **522**, 23–37 (2019).
43. C. B. Crawford, B. Quinn, Eds. *Microplastic Pollutants* (Elsevier Science, 2016).
44. W. Courtene-Jones, B. Quinn, C. Ewins, S. F. Gary, B. E. Narayanaswamy, Microplastic accumulation in deep-sea sediments from the Rockall Trough. *Mar. Pollut. Bull.* **154**, 111092 (2020).
45. I. A. Kane, M. A. Clare, E. Miramontes, R. Wogelius, J. J. Rothwell, P. Garreau, F. Pohl, Seafloor microplastic hotspots controlled by deep-sea circulation. *Science* **368**, 1140–1145 (2020).
46. K. R. Arrigo, D. K. Perovich, R. S. Pickart, Z. W. Brown, G. L. van Dijken, K. E. Lowry, M. M. Mills, M. A. Palmer, W. M. Balch, N. R. Bates, C. R. Benitez-Nelson, E. Brownlee, K. E. Frey, S. R. Laney, J. Mathis, A. Matsuoka, B. G. Mitchell, G. W. K. Moore, R. A. Reynolds, H. M. Sosik, J. H. Swift, Phytoplankton blooms beneath the sea ice in the Chukchi sea. *Deep Sea Res. Part II Top. Stud. Oceanogr.* **105**, 1–16 (2014).
47. M.-L. Timmermans, J. Marshall, Understanding Arctic Ocean circulation: A review of ocean dynamics in a changing climate. *J. Geophys. Res. Oceans* **125**, e2018JC014378 (2020).
48. J. Jung, K.-H. Cho, T. Park, E. Yoshizawa, Y. Lee, E. J. Yang, J.-K. Gal, S.-Y. Ha, S. Kim, S.-H. Kang, J. M. Grebmeir, Atlantic-origin cold saline water intrusion and shoaling of the nutricline in the Pacific Arctic. *Geophys. Res. Lett.* **48**, e2020GL090907 (2021).
49. P. Assmy, J. K. Ehn, M. Fernádez-Méndez, H. Hop, C. Katlein, A. Sundfjord, K. Bluhm, M. Daase, A. Engel, A. Fransson, M. A. Granskog, S. R. Hudson, S. Kristiansen, M. Nicolaus, I. Peeken, A. H. H. Enner, G. Spreen, A. Tatarek, J. Wiktor, Floating ice-algal aggregates below melting Arctic Sea ice. *PLOS ONE* **8**, e76599 (2013).
50. E. Yakushev, A. Gebruk, A. Osadchiev, S. Pakhomova, A. Lusher, A. Berezina, B. van Bavel, E. Vorozheikina, D. Chernykh, G. Kolbasova, I. Razgon, I. Semiletov, Microplastics distribution in the Eurasian Arctic is affected by Atlantic waters and Siberian rivers. *Commun. Earth Environ.* **2**, 23 (2021).
51. P. T. Harris, The fate of microplastic in marine sedimentary environments: A review and synthesis. *Mar. Polllut. Bull.* **158**, 111398 (2020).
52. P. G. Ryan, E. A. Weldeman, V. Perold, C. L. Moloney, Toward balancing the budget: Surface macro-plastics dominate the mass of particulate pollution stranded on beaches. *Front. Mar. Sci.* **7**, 575395 (2020).
53. Y. K. Song, S. H. Hong, S. Eo, M. Jang, G. M. Han, A. Isobe, W. J. Shim, Horizontal and vertical distribution of microplastics in Korean coastal waters. *Environ. Sci. Technol.* **52**, 12188–12197 (2018).
54. C. A. Choy, B. H. Robison, T. O. Gagene, B. Erwin, E. Firl, R. U. Halden, J. A. Hamilton, K. Katija, S. E. Lisin, C. Rolsky, K. S. van Houtan, The vertical distribution and biological transport of marine microplastics across the epipelagic and mesopelagic water column. *Sci. Rep.* **9**, 7843 (2019).
55. S. Eo, S. H. Hong, Y. K. Song, G. M. Han, S. Seo, W. J. Shim, Prevalence of small high-density microplastics in the continental shelf and deep sea waters of East Asia. *Water Res.* **200**, 117238 (2021).
56. K. Pabortsava, R. S. Lampitt, High concentrations of plastic hidden beneath the surface of the Atlantic Ocean. *Nat. Commun.* **11**, 4073 (2020).
57. L. D. K. Kanhai, K. Gårdfeldt, O. Lyashevska, M. Hassellöv, R. C. Thompson, I. O'Connor, Microplastics in sub-surface waters of the Arctic Central Basin. *Mar. Pollut. Bull.* **130**, 8–18 (2018).
58. P. S. Ross, S. Chastain, E. Vassilenko, A. Etemadifar, S. Zimmermann, S.-A. Quesnel, J. Eert, E. Solomon, S. Patankar, A. M. Posacka, B. Williams, Pervasive distribution of polyester fibres in the Arctic Ocean is driven by Atlantic inputs. *Nat. Commun.* **12**, 106 (2021).
59. C. Martin, F. Baalkhuyur, L. Valluzzi, V. Saderne, M. Cusack, H. Almahasheer, P. K. Krishnakumar, L. Rabaoui, M. A. Qurban, A. Arias-Ortiz, P. Masque, C. M. Duarté, Exponential increase of plastic burial in mangrove sediments as a major plastic sink. *Sci. Adv.* **6**, eaaz5593 (2020).
60. T. W. K. Armitage, G. E. Manucharyan, A. A. Petty, R. Kwook, A. F. Thompson, Enhanced eddy activity in the Beaufort Gyre in response to sea ice loss. *Nat. Commun.* **11**, 761 (2020).
61. M. M. R. van der Loeff, R. M. Key, J. Scholten, D. Bauch, A. Michel, $^{228}$Ra as a tracer for shelf water in the Arctic Ocean. *Deep Sea Res. Part II Top. Stud. Oceanogr.* **42**, 1533–1553 (1995).
62. A. A. Petty, J. K. Hutchings, J. A. Richter-Menge, M. A. Tschudi, Sea ice circulation around the Beaufort Gyre: The changing role of wind forcing and the sea ice state. *J. Geophys. Res. Oceans* **121**, 3278–3296 (2016).
63. A. Isobe, S. Iwasaki, K. Uchida, T. Tokai, Abundance of non-conservative microplastics in the upper ocean from 1957 to 2066. *Nat. Commun.* **10**, 417 (2019).
64. R. A. Woodgate, T. J. Weingartner, R. Lindsay, Observed increases in Bering Strait oceanic fluxes from the pacific to the arctic from 2001 to 2011 and their impacts on the Arctic Ocean water column. *Geophys. Res. Lett.* **39**, L24603 (2012).
65. Statista, Synthetic fiber production worldwide from 1940 to 2018 (2022); https://statista.-com/statistics/741368/world-synthetic-fiber-production/.
66. G. Suaria, A. Achtypi, V. Perold, J. R. Lee, A. Plerucci, T. G. Bornman, S. Allani, P. G. Ryan, Microfibers in oceanic surface waters: A global characterization. *Sci. Adv.* **6**, eaay8493 (2020).
67. J. A. Brandon, W. Jones, M. D. Ohman, Multidecadal increase in plastic particles in coastal ocean sediments. *Sci. Adv.* **5**, eaax0587 (2019).

68. F. Wania, A global mass balance analysis of the source of perfluorocarboxylic acids in the Arctic Ocean. *Environ. Sci. Technol.* **41**, 4529–4535 (2007).
69. M. B. Tekman, T. Krumpen, M. Bergmann, Marine litter on deep Arctic seafloor continues to increase and spreads to the North at the HAUSGARTEN observatory. *Deep Sea Res. Part I Oceanogr. Res. Pap.* **120**, 88–99 (2017).
70. K. B. P. Martínez, M. B. Tekman, M. Bergmann, Temporal trends in marine litter at three stations of the HAUSGARTEN Observatory in the Arctic deep sea. *Front. Mar. Sci.* **7**, 321 (2020).
71. P. E. Redondo-Hasselerharm, G. Gort, E. T. H. M. Peeters, A. A. Koelmans, Nano- and microplastics affect the composition of freshwater benthic communities in the long term. *Sci. Adv.* **6**, eaay4054 (2020).
72. A. Roach, K. Aagaard, C. Pease, S. Salo, T. Weingartner, V. Pavlov, M. Kulakov, Direct measurements of transport and water properties through the Bering Strait. *J. Geophys. Res. Oceans* **100**, 18443–18457 (1995).
73. W. B. Corlett, R. S. Pickart, The Chukchi slope current. *Prog. Oceanogr.* **153**, 50–65 (2017).
74. J. Masura, J. Baker, G. Foster, C. Arthur, "Laboratory methods for the analysis of microplastics in the marine environment: Recommendations for quantifying synthetic particles in waters and sediments" (NOAA Technical Memorandum NOS-OR&R-48, NOAA, 2015).
75. S. L. Wright, J. Ulke, A. Font, K. L. A. Chan, F. J. Kelly, Atmospheric microplastic deposition in an urban environment and an evaluation of transport. *Environ. Int.* **136**, 105411 (2020).
76. R. Pirtle-Levy, J. M. Grebmeier, L. W. Cooper, I. L. Larsen, Chlorophyll *a* in Arctic sediments implies long persistence of algal pigments. *Deep Sea Res. Part II Top. Stud. Oceanogr.* **56**, 1326–1338 (2009).
77. J.-H. Kim, J.-K. Gal, S.-Y. Jun, L. Smik, D. Kim, S. T. Belt, K. Park, K.-H. Shin, S.-I. Nam, Reconstructing spring sea ice concentration in the Chukchi Sea over recent centuries: Insights into the application of the $PIP_{25}$ index. *Environ. Res. Lett.* **14**, 125004 (2019).
78. M. Poulain, M. J. Mercier, L. Brach, M. Martignac, C. Routaboul, E. Perez, M. C. Desjean, A. Halle, Small microplastics as a main contributor to plastic mass balance in the North Atlantic subtropical gyre. *Environ. Sci. Technol.* **53**, 1157–1164 (2019).
79. A. W. Nolin, R. Armstrong, J. Maslanik, "Near-Real-Time SSM/I-SSMIS EASE-Grid Daily Global Ice Concentration and Snow Extent, version 4" (NASA National Snow and Ice Data Center Distributed Active Archive Center, 1998).
80. M. J. Brodzik, J. S. Stewart, "Near-Real-Time SSM/I-SSMIS EASE-Grid Daily Global Ice Concentration and Snow Extent, version 5, (NASA National Snow and Ice Data Center Distributed Active Archive Center, 2016).
81. J. Boucher, D. Friot, Primary microplastics in the oceans: A global evaluation of sources. IUCN available at https://portals.iucn.org/library/sites/library/files/documents/2017-002.pdf.


**Acknowledgments:** This study is the outcome of the IBRV *Araon* R/V expedition. We thank the captain and crew of R/V *Araon* for their assistance with sample collection. We thank K.-H. Cho for ice map. **Funding:** This work was supported by the Basic Science Research Program (no. 2017R1E1A1A01073137) and R&D Program for Oceans and Polar Regions (no. 2019M1A5A1101471) of the National Research Foundation of Korea (NRF) funded by the Ministry of Science and ICT (MSIT), Republic of Korea. This work was also supported by "Korea-Arctic Ocean Warming and Response of Ecosystem, KOPRI (no. 20210605)" and by "Land/Sea-based input and fate of microplastics in the marine environment (no. 20220357)" of Korea Institute of Marine Science & Technology Promotion (KIMST) funded by the Ministry of Oceans and Fisheries, Republic of Korea. **Author contributions:** S.-K.K. led the research design, data collection, field sampling, interpretation of results, and writing of the manuscript; J.-S.K., S.-Y.K., and H.S.L. collected samples during the R/V expedition; S.-Y.K. and E.J.Y. provided aging data of the sediment core and environmental variable analysis data; N.-S.S. analyzed MPs in Arctic samples; and S.-K.K. wrote the manuscript with contributions from all coauthors. **Competing interests:** The authors declare that they have no competing interests. **Data and materials availability:** All data needed to evaluate the conclusions in the paper are present in the paper and/or the Supplementary Materials.

Submitted 29 May 2022
Accepted 31 May 2023
Published 5 July 2023
10.1126/sciadv.add2348